Cell Reports

Article

Fc-mediated pan-sarbecovirus protection after alphavirus vector vaccination

Graphical abstract

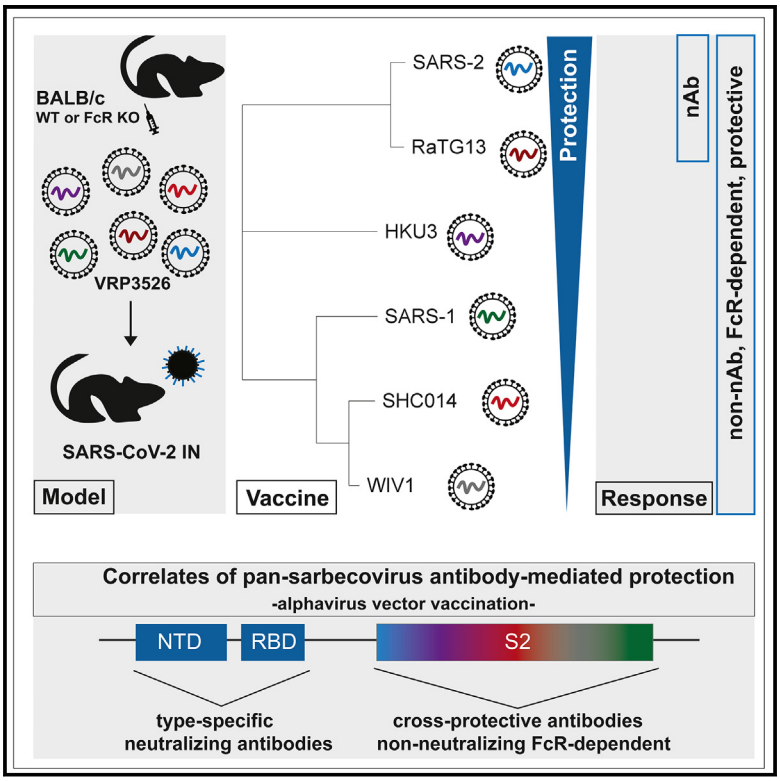

Highlights

- Non-neutralizing antibodies mediate pan-sarbecovirus protection
- Antibody-mediated cross-protection is lost in absence of FcR function
- S2-specific antibodies are a strong correlate of protective FcR effector function
- Full-length spike elicits the broadest pan-sarbecovirus protection

Authors

Lily E. Adams, Sarah R. Leist, Kenneth H. Dinnon III, ..., Victoria K. Baxter, Mark T. Heise, Ralph S. Baric

Correspondence

mark_heisem@med.unc.edu (M.T.H.), rbaric@email.unc.edu (R.S.B.)

In brief

Using a lethal model for β-coronavirus infection, Adams et al. described heterologous protection from disease that was driven by non-neutralizing antibodies through Fc-receptor-dependent mechanisms. These results reveal important protective correlates for inclusion into the design and testing of future pan-coronavirus vaccines.

Adams et al., 2023, Cell Reports *42*, 112326
April 25, 2023
https://doi.org/10.1016/j.celrep.2023.112326

CellPress

Cell Reports

CellPress
OPEN ACCESS

Article

Fc-mediated pan-sarbecovirus protection after alphavirus vector vaccination

Lily E. Adams,[1,10] Sarah R. Leist,[2] Kenneth H. Dinnon III,[1] Ande West,[2,4] Kendra L. Gully,[2,3] Elizabeth J. Anderson,[3] Jennifer F. Loome,[1] Emily A. Madden,[1] John M. Powers,[2] Alexandra Schäfer,[2] Sanjay Sarkar,[4] Izabella N. Castillo,[1] Jenny S. Maron,[7] Ryan P. McNamara,[7] Harry L. Bertera,[7] Mark R. Zweigert,[2] Jaclyn S. Higgins,[1] Brea K. Hampton,[4] Lakshmanane Premkumar,[1] Galit Alter,[7] Stephanie A. Montgomery,[5,8] Victoria K. Baxter,[3,5,9] Mark T. Heise,[1,4,6,9,*] and Ralph S. Baric[1,2,6,9,*]

[1]Department of Microbiology and Immunology, University of North Carolina at Chapel Hill, Chapel Hill, NC, USA
[2]Department of Epidemiology, University of North Carolina at Chapel Hill, Chapel Hill, NC, USA
[3]Division of Comparative Medicine, University of North Carolina at Chapel Hill, Chapel Hill, NC, USA
[4]Department of Genetics, University of North Carolina at Chapel Hill, Chapel Hill, NC, USA
[5]Department of Pathology and Laboratory Medicine, University of North Carolina at Chapel Hill, Chapel Hill, NC, USA
[6]Rapidly Emerging Antiviral Drug Discovery Initiative, University of North Carolina at Chapel Hill, Chapel Hill, NC, USA
[7]Ragon Institute of MGH, MIT, and Harvard University, Cambridge, MA, USA
[8]Dallas Tissue Research, Dallas, TX, USA
[9]Senior author
[10]Lead contact
*Correspondence: mark_heisem@med.unc.edu (M.T.H.), rbaric@email.unc.edu (R.S.B.)
https://doi.org/10.1016/j.celrep.2023.112326

SUMMARY

Group 2B β-coronaviruses (sarbecoviruses) have caused regional and global epidemics in modern history. Here, we evaluate the mechanisms of cross-sarbecovirus protective immunity, currently less clear yet important for pan-sarbecovirus vaccine development, using a panel of alphavirus-vectored vaccines covering bat to human strains. While vaccination does not prevent virus replication, it protects against lethal heterologous disease outcomes in both severe acute respiratory syndrome coronavirus 2 (SARS-CoV-2) and clade 2 bat sarbecovirus challenge models. The spike vaccines tested primarily elicit a highly S1-specific homologous neutralizing antibody response with no detectable cross-virus neutralization. Rather, non-neutralizing antibody functions, mechanistically linked to FcgR4 and spike S2, mediate cross-protection in wild-type mice. Protection is lost in FcR knockout mice, further supporting a model for non-neutralizing, protective antibodies. These data highlight the importance of FcR-mediated cross-protective immune responses in universal pan-sarbecovirus vaccine designs.

INTRODUCTION

β-Coronaviruses (β-CoVs) have caused epidemic and pandemic disease in human populations in the twenty-first century. The 2002 severe acute respiratory coronavirus (SARS-CoV) and the 2019 SARS-CoV-2 represent prototype clade 1a and clade 1b group 2B β-CoV strains, belonging to subgenus sarbecovirus. SARS-CoV and SARS-CoV-2 likely emerged from bat reservoirs either through intermediate host transmission events or through direct spread into human populations.[1,2] The subgenus includes other highly heterogeneous epidemic, pandemic, and zoonotic strains poised for emergence, such as SHC014 and WIV1, which replicate efficiently in primary human cells and human ACE2 transgenic mice.[3–11] The accelerated approval of SARS-CoV-2 vaccines is the result of decades of basic and applied research.[12] However, current SARS-CoV-2 spike-based vaccines provide limited protection against heterologous bat sarbecoviruses, as well as recently emerged SARS-CoV-2 variants of concern (VOCs).[13] The complex immunologic mechanisms regulating cross-protection against closely related and distant strains is critical for pan-CoV vaccine design and public health preparedness.

The sarbecovirus spike glycoprotein is a trimeric class I viral fusion protein of roughly 1,300 amino acids. Spike is divided into an amino-terminal S1 subunit and a carboxy-terminal S2 subunit that drives membrane fusion. The S1 subunit is further subdivided into a highly variable N-terminal domain (NTD) and a receptor-binding domain (RBD), which engages the ACE2 receptor. Subtle molecular communication networks across domains are thought to influence epitope presentation and likely vaccine cross-protection.[14,15] Recent work characterizing immunity against distinct spike proteins following homologous or heterologous vaccination identified broadly conserved epitopes across SARS-CoV-2 and divergent CoVs.[16–19] However, the role of these epitopes in protective immunity remains under investigation.[17,20,21] After SARS-CoV-2 natural infection or vaccination, the spike RBD, NTD, and S2 domains stimulate neutralizing and non-neutralizing antibody responses. Among sarbecoviruses, broadly protective neutralizing antibodies primarily target

specific epitopes of the spike glycoprotein,[18,22–27] typically in the RBD.[28,29] However, neutralizing antibody potency *in vitro* and protective function do not always correlate *in vivo*.[29] Further, several studies have shown that antibody FcR-mediated effector functions are critical in protective immunity.[30–34] Fc receptors have high affinity for immunoglobulin (Ig) G subtypes and are cell surface receptors on monocytes, macrophages, neutrophils, and other immune cells; FcR recognition of the antibody Fc region stimulates effector cell function such as NK cell-mediated lysis, neutrophil degranulation, and antibody-dependent cellular phagocytosis (ADCP).[35] Thus, FcR effector function may be a key protective correlate for next-generation vaccine development and improvement.

Here, we used a Venezuelan equine encephalitis virus 3526 replicon particle (VRP3526)[36] to evaluate mechanisms of cross-protection after pandemic and pre-emergent CoV spike glycoprotein vaccination in mice, followed by lethal CoV challenge.[37–39] Here, contemporary human CoV spikes elicited no protection, and SARS-CoV-2 spike vaccines protected against weight loss, lethal disease, and virus replication after SARS-CoV-2 challenge. In contrast, heterologous VRP sarbecovirus spike vaccines conferred cross-protection against weight loss and death but provided limited but significant reductions in virus replication in young and aged animals. Homologous protection correlated with potent neutralizing antibody responses that principally targeted the S1 subdomains, but few if any cross-neutralizing antibodies were detected against the heterologous sarbecovirus strains after low vaccine dose. Rather, systems serology,[40] *in vitro* studies, and passive antibody transfer experiments in wild-type and Fc-receptor-deficient mice implicated an FcR-driven mechanism targeting S2, such as ADCP. These results build support for universal sarbecovirus vaccine designs that couple FcR-mediated cross-protection, with potent cross-neutralizing antibody responses.

RESULTS

Sarbecovirus VRP35226 spike vaccine designs

VRP3526 replicon particles, which are non-select agent, replication-deficient vaccine vectors derived from a live attenuated strain, were assembled as previously described[36] (Figure 1A). We generated VRPs expressing spike proteins from α- and β-CoVs, including three common-cold CoVs, OC43, NL63, and HKU1 (Figure 1B, green), as well as epidemic and/or pandemic (SARS-CoV, SARS-CoV-2) and pre-emergent sarbecoviruses circulating in animal reservoirs (RaTG13, HKU3, WIV1, SHC014) (Figure 1B, red). The sarbecovirus spike glycoproteins were separated into three groups based on amino acid similarity: clade 1a (SARS-CoV, SHC014, WIV1), 2 (HKU3), and 1b (SARS-CoV-2, RaTG13) (Figure 1A).[41] The clade 1b virus RaTG13 spike protein is 97.4% identical to the SARS-CoV-2 spike protein, while the clade 2 virus HKU3 and clade 1a virus spike proteins share 75.6%–78.6% identity to the SARS-CoV-2 spike protein. Clade 2 HKU3 spike protein shares 78.1%–78.8% identity to the clade 1a spike proteins (Figure 1D). All VRP titers exceeded 2×10^6 IU/mL (Figure 1C).[36] S2 immunofluorescent staining for the highly conserved spike S2 domain verified spike expression in mammalian cells infected by VRPs (Figure 1D).

VRP-vectored spike proteins protect against severe SARS-CoV-2 disease in young mice

To test the VRP3526 platform's ability to elicit cross-protection, we employed a lethal mouse model for SARS-CoV-2 disease. Groups (n = 8–10) of 8- to 10-week-old female BALB/cAnNHsd (BALB/c) mice were vaccinated with a dose of 2×10^4 IU VRP encoding each of the different spike vaccines by footpad injection, as this route induces robust mucosal immunity,[36] then boosted on day 21 with the homologous spike VRP. As shown previously[42] and in Figure 2, relatively low doses of VRP spike vaccines will elicit complete homologous protection while providing an expanded phenotypic window to examine cross-protection. At 21 days post-boost (now aged 14–16 weeks), mice were challenged with 10^4 plaque-forming units (PFUs) SARS-CoV-2 MA10 (MA10)[42] intranasally. Virus titer in the lungs after challenge is a sensitive measure of vaccine performance,[12,43] and only the VRP SARS-CoV-2 spike vaccine elicited nearly complete protection from homologous virus lung replication. In contrast, the clade 1b VRP RaTG13 spike vaccination caused slight but significant reductions in virus titers on day 2 (1-log) and 5 (3-log) post-infection, compared with the GFP-vaccinated controls. In clade 2 VRP HKU3 spike-vaccinated animals, MA10 titers were also significantly reduced by about 1.5 and 3 logs on days 2 and 5 post-infection. The most heterogeneous clade 1a vaccines (SARS-CoV, WIV1, and SHC014) were least effective and reduced titers by ~2 logs on day 5 post-infection (Figure 2A).

Bronchoconstriction and airway resistance in the lungs of challenged mice, measured by whole-body plethysmography, mirrors some human disease phenotypes.[44] Calculating area under the curve (AUC), we found that clade 1b and clade 2 vaccines effectively protected against bronchoconstriction (Rpef) and airway resistance (PenH) after SARS-CoV-2 MA10 challenge (Figure 2B), accordant with reduced clinical disease. In contrast, clade 1a vaccinated animals had significantly increased respiratory dysfunction and clinical disease, indicative of reduced lung function. In parallel, we monitored weight loss and assessed lung pathology by scoring gross discoloration (GLD), diffuse alveolar damage (DAD), and acute lung injury (ALI) following MA10 challenge. Homologous challenge in VRP SARS-CoV-2 spike-vaccinated animals resulted in minimal weight loss (Figure 2C) and GLD (Figure 2F), reflecting protection from significant SARS-CoV-2 disease. In contrast, the zoonotic and pandemic CoV spike vaccines partially protected from clinical disease. For example, the clade 1b CoV spike vaccines protected against severe SARS-CoV-2 disease, resulting in little (~10% RaTG13) to no measurable weight loss (SARS-CoV-2) and minimal GLD at the time of tissue harvest (Figures 2C and 2F). Under identical conditions, clade 1a spike (SARS-CoV, WIV1, and SHC014) vaccines elicited low-level intermediate protection after MA10 challenge, resulting in 10%–15% body weight lost and notable increases in GLD (Figures 2E and 2F). Despite being as distant as the clade 1a CoV spikes from the SARS-CoV-2 spike and containing deletions in the NTD and RBD (Figures 1 and S1), the clade 2 HKU3 spike vaccine elicited near-full protection against disease with ~5% weight loss and minimal GLD (Figures 2D and 2F). Thus, the protection elicited by VRP HKU3 spike after MA10 heterologous challenge is particularly noteworthy. Within spike

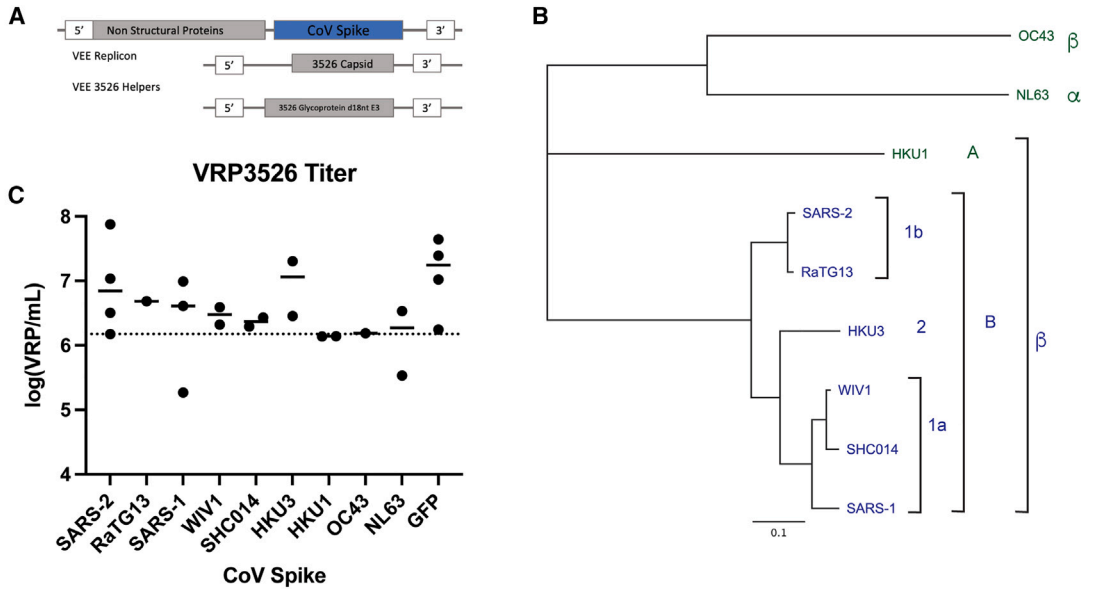

D

	SARS-CoV-2	RaTG13	SARS-CoV	SHC014	WIV1
RaTG13	97.4 | 0.023				
SARS-CoV	75.6 | 0.248	76.2 | 0.247			
SHC014	76.8 | 0.246	77.0 | 0.245	90.0 | 0.099		
WIV1	76.5 | 0.233	77.0 | 0.232	92.3 | 0.086	97.1 | 0.030	
HKU3	75.8 | 0.248	76.0 | 0.247	78.1 | 0.225	78.8 | 0.223	78.8 | 0.210

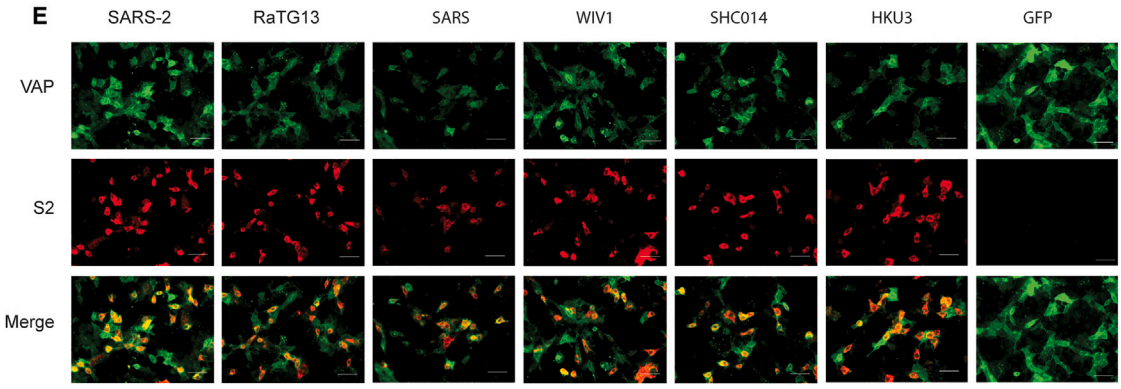

Figure 1. Venezuelan equine encephalitis virus replicon particle VRP3526 for high-titer vaccinations

(A) Venezuelan equine encephalitis (VEE) RNA-based assembly scheme of VRP3526 particles.

(B) Phylogenetic relationship of the spike protein amino acid sequences from CoVs that were used in this study, including common cold CoVs (green) and prepandemic/epidemic CoVs (blue). Of the β-CoVs, we generated spike proteins for both group 2A (HKU1) and 2B viruses. Of the group 2B viruses, we generated spike proteins for clade 1a (SARS-CoV, SHC014, WIV1), 2 (HKU3), and 1b (SARS-CoV-2, RaTG13) viruses. Tree generated from an amino acid multiple sequence alignment using maximum likelihood in Geneious Prime.

(C) VRP3526 titers obtained in this study. Dashed line denotes minimum titer required for vaccination at 2×10^4 VRPs in a 10-μL footpad inoculation.

(D) Amino acid percentage similarity (left in cell) and patristic phylogenetic distance (right in cell) of the main sarbecovirus spike proteins used in this study.

(E) Immunofluorescent staining at 40× magnification for VEE non-structural proteins (top) and SARS-CoV-2 spike S2 domain (middle) in Vero E6 cells infected with VRPs expressing the spike proteins used in this study. White scale bar, 50 μm.

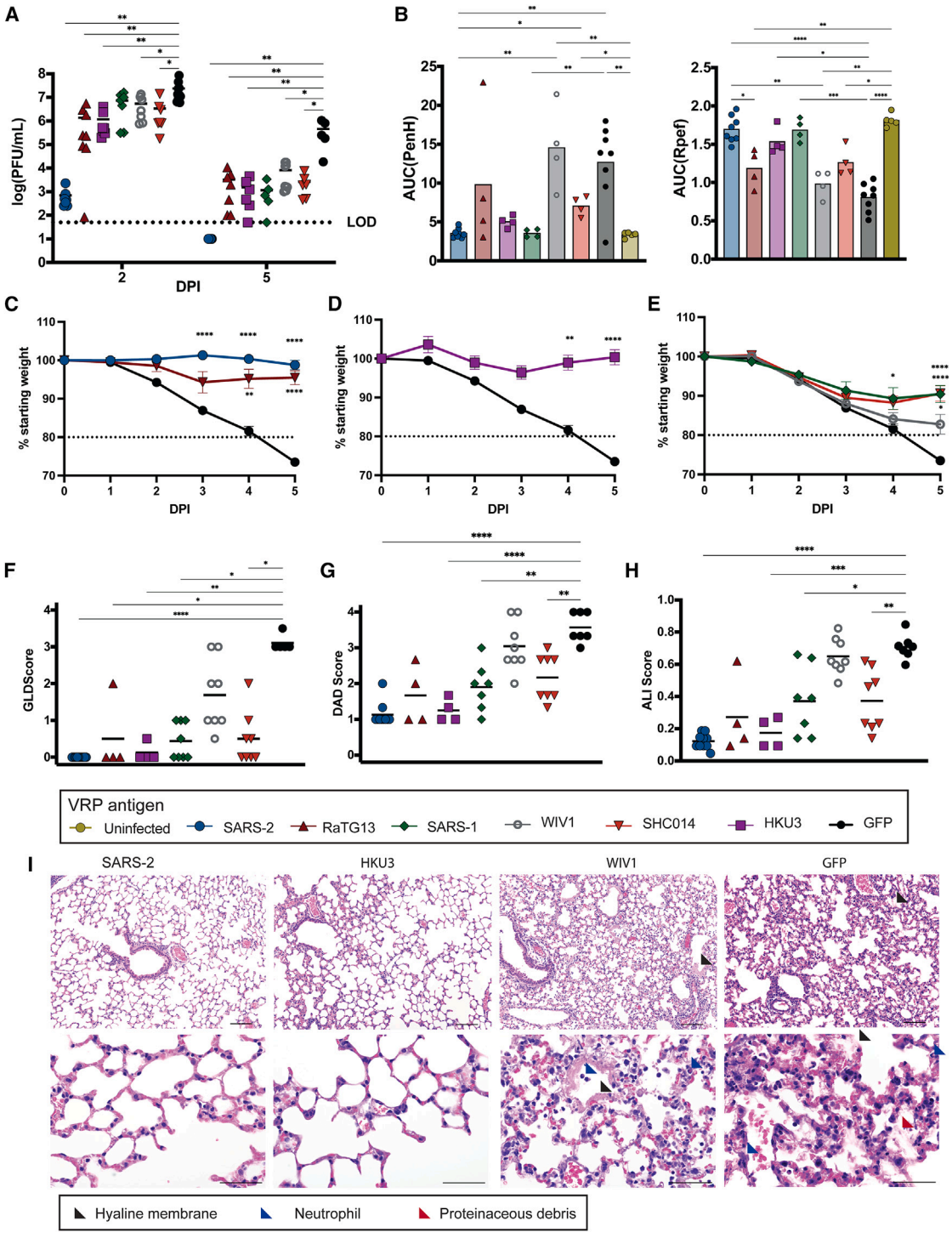

Figure 2. VRP sarbecovirus spike vaccines elicit a cross-protective immune response against SARS-CoV-2

(A) SARS-CoV-2 lung titer calculated via plaque assay on days 2 and 5 post-infection. Samples that fell below the limit of detection (dotted line) were set to 25 PFU/mL.

(B) Area under the curve (AUC) of lung function metrics of airflow resistance (PenH, right) and bronchoconstriction (Rpef, left). Lung function was measured by BUXCO whole-body plethysmography (WBP) systems one each experimental day; AUC calculated for time course of each mouse.

(C–E) Body weights calculated after infection of 10^4 PFU SARS-CoV-2 intranasally through the duration of the experiment on animals vaccinated with clade 1b I, 2 (D), and I (E) sarbecovirus spike proteins. Data were pooled from three independent studies. n = 4 mice followed to study endpoint for body weights (C) and lung function (B) from each vaccine group for each experiment, resulting in n = 4 reported for spike vaccines and n = 8 reported for VRP GFP (comprising two

(legend continued on next page)

vaccine groups where mice were partially protected from disease by weight loss and GLD (e.g., WIV1, SHC014), outcomes ranged from mild to severe, suggesting that this protective mechanism is subject to strain-specific spike variation. Using the data from the pooled studies, we calculated Pearson product-moment correlation coefficients between each metric to measure the linear associations between the data. Using this analysis, we calculated a robust and significant negative correlation coefficient (-0.76, $p < 0.0001$) between GLD and body weight maintenance weight as well as a strong, significant positive correlation (0.72, $p < 0.0001$) between virus titers on day 2 and day 5 post-infection (Figure S2G). Moreover, a significant negative correlation coefficient (-0.68, $p < 0.0001$) between viral titer 2 days post infection (DPI) and body weight maintenance suggested virus titer may be predictive of disease severity in our model.

Consistent with prior studies,[42] histological examination (Figures 2G and 2H) at day 5 post-infection identified severe disease signs in infected control animals, including infiltration of neutrophils in the interstitial and alveolar spaces, alveolar septal thickening, cell sloughing and proteinaceous debris in the airspaces, and hyaline membrane formation consistent with DAD and ALI phenotypes[42] (Figure 2I, red, blue, black). In contrast, mice vaccinated with the homologous spike demonstrated significant protection from SARS-CoV-2-induced lung pathology, with baseline-equivalent DAD and ALI scores (41) (Figures 2G–2I). Heterologous vaccines that were associated with greater GLD scores and thus only partial protection (e.g., WIV1) demonstrated elevated DAD and ALI scores compared with the SARS-CoV-2 vaccine group, although they were significantly reduced compared with infected control animals. Vaccines that were more protective (e.g., HKU3) resulted in significantly lower DAD and ALI scores, comparable with the SARS-CoV-2 spike-vaccinated group.

We also used the MA10 challenge model to evaluate whether vaccination with VRPs expressing spikes of contemporary common cold human β-CoV, which share conserved S2 epitopes with epidemic and pre-emergent β-CoV,[45,46] would protect against SARS-CoV-2 disease. We found that single exposures (single component, two doses) of contemporary human CoV spike vaccines did not protect against severe SARS-CoV-2 disease and mortality in young mice (Figures S2A and S2C), nor did these vaccines reduce viral replication efficiency (Figure S2B). In contrast to the Group 2B CoV-vaccinated mice, a large percentage (>50% in most cases) of common cold spike-vaccinated mice died or lost >20% body weight and were euthanized compared with those vaccinated with VRP SARS-CoV-2 spike (Figure S2C).

Evaluating the potential for aberrant immunity after vaccination is especially important as killed/inactivated CoV vaccines have been reported to induce a pro-inflammatory and Th2 skewed immune response commonly associated with immune pathology.[43,47] Using a BioPlex cytokine immunoassay, we measured the cytokine responses after challenge in vaccinated mice on days 2 and 5 post-infection. We did not detect elevated T helper (Th) 2 cell cytokine signatures (interleukin [IL]-4, IL-5, IL-13) in vaccinated mice on day 2 or 5, but a strong Th1 signature (significant increases in IL-12, tumor necrosis factor [TNF]-α, interferon [IFN]-γ) was commonly associated with a protective immune response.[36] In contrast to the groups vaccinated with the homologous SARS-CoV-2 spike, groups vaccinated with the heterologous sarbecovirus VRP spikes also demonstrated elevated pro-inflammatory cytokine responses in the lung 2 days post-MA10 challenge (IL-1β, IFN-γ, TNF-α, IL-6) (Figure S3). Altogether, this suggests the VRP sarbecovirus spike vaccines elicited a protective immune response against SARS-CoV-2 infection.

VRP-vectored spike proteins protect against severe SARS-CoV-2 disease in aged mice

To evaluate the potential for cross-protection in an aging population, we utilized the MA10 lethal challenge model in aged (1 year old) mice. Mice were immunized and 3 weeks post-boost were challenged with 10^3 PFUs (~1 median lethal dose [LD_{50}], typically >20% weight loss) MA10 intranasally (Figures 3A–3F). In our homologous vaccinated, aged mouse model, mice challenged with MA10 experienced ~5% weight loss before recovery (Figure 3A). Importantly, VRP SARS-CoV-2 spike-vaccinated animals were also significantly protected from GLD (Figure 3D) and virus titers on day 2 and 5, respectively (Figure 3E). In addition, clade 1b VRP RaTG13 and clade 2 VRP HKU3 spike-vaccinated animals showed limited weight loss (~8%–10%) and GLD on days 2 and 5 post-infection (Figures 3A and 3D). Clade 2 VRP HKU3 spike-vaccinated animals also displayed significant reductions in virus titer on days 2 and 5 post-infection. However, the aged mice vaccinated with VRP RaTG13 or VRP HKU3 were less protected than similarly vaccinated young mice by both weight loss (Figures 3A, 3B, 2C, and 2D) and GLD (Figures 3D and 2F), which is consistent with the enhanced susceptibility and reduced vaccine efficacy seen during sarbecovirus challenge of aged mice.[42,47] Clade 1a VRP spike vaccines elicited variable levels of protection in the aged mouse model after MA10 challenge (Figures 3B and 3D). Clade 1a VRP vaccines were the least protective against weight loss and GLD (Figures 3C and 3D), and VRPs WIV1 and SHC013 did not prevent virus replication. Reductions in respiratory function generally correlated with overall disease severity, as measured by

experiments). n = 4–10 were evaluated for GLD (F), DAD (G), and ALI (H) score. n = 8–10 mice evaluated at day 2 post-infection for virus titer (A). Reported as percentage of starting weight. Horizontal line indicates 20% body weight lost and animal care humane endpoint.

(F–H) (F) Semi-quantitative gross lung discoloration (GLD) scoring, (G) Diffuse alveolar damage (DAD) scoring, and (H) acute lung injury (ALI) scoring upon tissue harvest at day 5 post-infection (5 DPI).

(I) Hematoxylin and eosin-stained sections of lungs from vaccinated mice harvested day 5 post-infection. Black arrow, hyaline membrane; blue arrow, neutrophil infiltrate; red arrow, proteinaceous debris. Top: 100× magnification; black scale bar, 100 μm. Bottom: 400× magnification, black scale bar, 50 μm. Mean data points, arithmetic mean; error bars, standard error from the mean. Significance calculations: weight loss, two-way ANOVA; weight loss in cases of mortality, mixed-effects analysis; virus titer, one-way ANOVA; GLD and lung damage scoring, Brown-Forsythe and Welch's ANOVA; lung function (WBP), Kruskal-Wallis test corrected by Dunn's multiple comparisons; all other corrections, Dunnett's, T3 when total samples <50. *$p < 0.05$, **$p < 0.01$, ***$p < 0.001$, ****$p < 0.0001$.

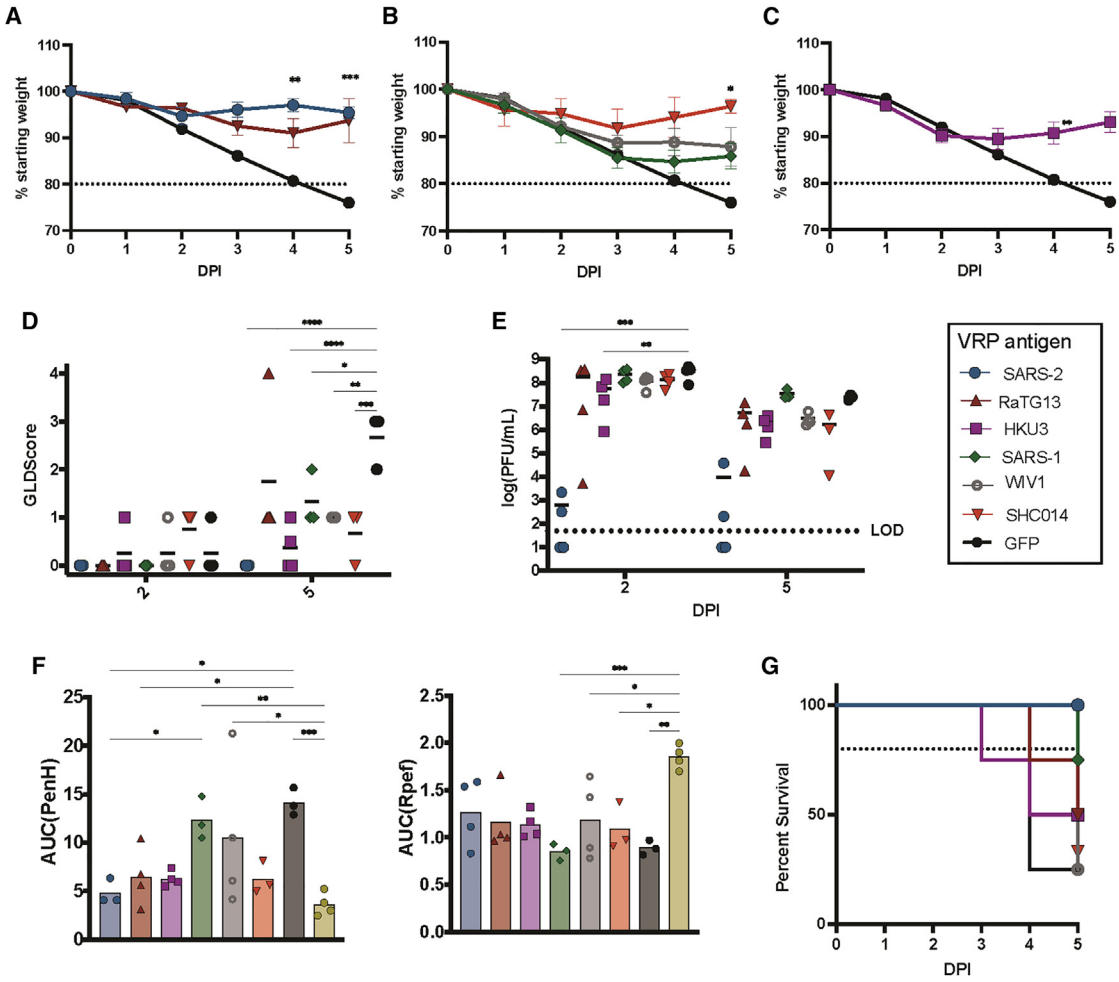

Figure 3. VRP spike protects from lethal infection in vulnerable aged mice. Old mice (12 months) were challenged with 10^3 PFU SARS-CoV-2 MA10 intranasally unless otherwise noted

(A–C) Body weights calculated through the duration of the experiment on animals vaccinated with clade 1b (A), 2 (B), and 1a (C) sarbecovirus spike proteins. Reported as percentage of starting weight. Horizontal line indicates 20% body weight lost and animal care humane endpoint.

(D) GLD scoring upon tissue harvest.

(E) SARS-CoV-2 lung titer calculated via plaque assay. Samples that fell below the limit of detection (dotted line) were set to 25 PFU/mL.

(F) AUC of lung function metrics of airflow resistance (PenH, right) and bronchoconstriction (Rpef, left). Lung function was measured by BUXCO WBP systems one each experimental day, AUC calculated for time course of each mouse.

(G) Survival of vaccinated animals when challenged with 10^4 PFU SARS-CoV-2 MA10 intranasally. Data are representative of one study, with n = 4 mice reported for each harvest day and n = 4 mice followed to study endpoint. Mean data points, arithmetic mean; error bars, standard error from the mean. Significance calculations: weight loss, two-way ANOVA; weight loss in cases of mortality, mixed-effects analysis; virus titer, one-way ANOVA; GLD scoring, Brown-Forsythe and Welch's ANOVA; lung function (WBP), Kruskal-Wallis test corrected by Dunn's multiple comparisons; all other corrections, Dunnett's, T3 when total samples <50. *p < 0.05, **p < 0.01, ***p < 0.001, ****p < 0.0001.

weight loss and GLD (Figure 3F). Compared with young mice, MA10 replicated to higher titers in the lungs of the old mice with more breakthrough replication in the homologous vaccinated mice (Figure 3E), reflecting the age-associated reduction in vaccine efficacy seen in this model.[42,47]

As aged animals are significantly more vulnerable to higher MA10 challenge doses,[42] we next determined whether the VRP sarbecovirus spike vaccine panel could protect against a 10-fold higher, 10^4 challenge dose, which typically results in 85% mortality. Mice vaccinated with VRP SARS-CoV-2 spike were fully protected from severe disease and mortality through day 5 post-infection. In contrast, mice vaccinated with other clade 1a, 1b, or clade 2 heterologous VRP spike vaccines experienced equivalent weight loss to mock-vaccinated controls (Figures S2D–S2F) and high mortalities of 25%–75% (Figure 3G), indicating the cross-protection in our model has dramatic potential to vary in an aging population.

VRP SARS-CoV-2 spike protects against disease in heterologous sarbecovirus infection

Recent studies suggest that some clade 2 strains can use bat ACE2 molecules for entry if isolated from their natural bat host

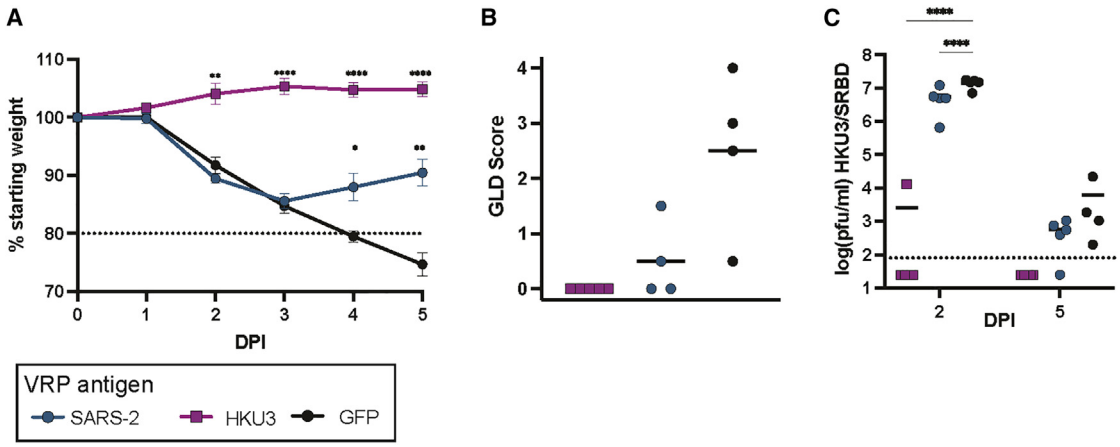

Figure 4. VRP SARS-CoV-2 spike vaccination protects against heterologous challenge

Young mice (16–18 weeks) were challenged with 10^5 PFU HKU3/SRBD MA intranasally.

(A) Body weights calculated through the duration of the experiment on animals vaccinated with SARS-CoV-2 or HKU3 spike proteins, or vectored GFP.

(B) Semi-quantitative macroscopic lung discoloration scoring upon tissue harvest.

(C) HKU3 lung titer calculated via plaque assay. Body weights reported as percentage of starting weight where horizontal line indicates 20% body weight lost and animal care humane endpoint. Titer samples that fell below the limit of detection (dotted line) were set to 25 PFU/mL. Data are representative of one study, with n = 4 mice reported for each harvest day and n = 4 mice followed to study endpoint. Mean data points, arithmetic mean; error bars, standard error from the mean. Significance calculations: weight loss, two-way ANOVA; weight loss in cases of mortality, mixed-effects analysis; virus titer, one-way ANOVA; GLD scoring, Brown-Forsythe and Welch's ANOVA; all corrections, Dunnett's, T3 when total samples <50. *p < 0.05, **p < 0.01, ***p < 0.001, ****p < 0.0001.

species,[11,48] which suggests clade 2 sarbecoviruses may threaten global health. Importantly, the antigenically distant HKU3 spike (Figure 1) vaccine protected against MA10 disease (Figure 2). As HKU3 could emerge by mutation or RNA recombination, we next evaluated whether the VRP SARS-CoV-2 spike vaccine would protect against clade 2 heterologous challenge. Eight- to 10-week-old mice were vaccinated and boosted with VRP HKU3 spike, VRP SARS-CoV-2 spike, and VRP GFP vaccines as previously described. Vaccinated mice were then infected intranasally with the mouse-adapted clade 2 bat sarbecovirus designated HKU3-SRBD MA, which causes disease in mice.[11,49] The homologous HKU3 spike-vaccinated animals were fully protected from weight loss and GLD and showed a significant 4-log reduction in titer after HKU3-SRBD challenge (Figures 4A–4C). In contrast, the heterologous VRP SARS-CoV-2 spike vaccine attenuated HKU3-SRBD disease severity, as shown by ~15% body weight loss (Figure 4A) and modest reductions in GLD (Figure 4B). Modest but significant ~5- and 10-fold reductions in virus titer were also noted on days 2 and 5 post-infection, respectively, in VRP SARS-CoV-2 spike-vaccinated mice (Figure 4C). The cross-protective phenotype mediated by VRP spike vaccines in two unique challenge models prompted further mechanistic investigation.

VRP spike vaccinations induce non-neutralizing, cross-reactive antibodies

To evaluate the antibody response elicited by the VRP vaccines in young animals, we measured total spike binding and neutralizing antibody response in vaccine sera prior to challenge with SARS-CoV-2 (Figure 2). Each VRP spike vaccine elicited a potent serologic (cross-reactive) IgG response against the SARS-CoV-2 spike protein (Figure 5A, left). We observed total IgG titers of 10^4 as well as a potent IgG response against the SARS-CoV-2 receptor-binding domain (RBD; Figure 5A, middle). Mice vaccinated with VRP RaTG13 did not produce significant IgG against the SARS-CoV-2 RBD, despite inducing notable IgG against the SARS-CoV-2 N-terminal domain, comparable with the homologous VRP SARS-CoV-2 vaccine (NTD; Figure 5A, right). Supporting this result, NTD is well conserved between SARS-CoV-2 and RaTG13 (98.3% amino acid identity), while the RBD is more diverged (89.3%). We detected a strong IgG2a skew in VRP spike antigen-vaccinated mice (Figure 5B), further suggesting that vaccination induced a protective Th1 response.[50] We also observed a marked vaccine antigen-specific grouping in the ratio of IgG2a to IgG1, and further analyses demonstrated high reactivity toward full-length spike with little to no preference for IgG2a recognition of S1 or S2 (Figure 5C).

Via a series of live-virus assays, we characterized the neutralizing antibody response. At our vaccine dose, we detected neutralizing antibodies in mice vaccinated with VRP SARS-CoV-2 with a half maximal inhibitory concentration (IC_{50}) of ~1:700 but did not detect potent cross-neutralizing antibody responses in mice vaccinated with heterologous VRP spikes toward luciferase reporter SARS-CoV-2 (Figure 5D). Further, VRP SHC014 sera neutralized reporter virus SHC014 with an IC_{50} of ~1:800 (Figure 5F), but there was also no detectable neutralization of the SHC014 virus by VRP SARS-CoV-2 sera. Using a luciferase reporter system to detect spike NTD, RBD, and S1 domain-specific neutralizing antibodies,[13,29] we determined that the majority of VRP SARS-CoV-2 spike-neutralizing antibodies targeted the RBD (amino acids 332–528) and the C-terminal segment of S1 (RBD+, amino acids 332–685). Additionally, the VRP SARS-CoV-2 spike vaccines failed to elicit measurable

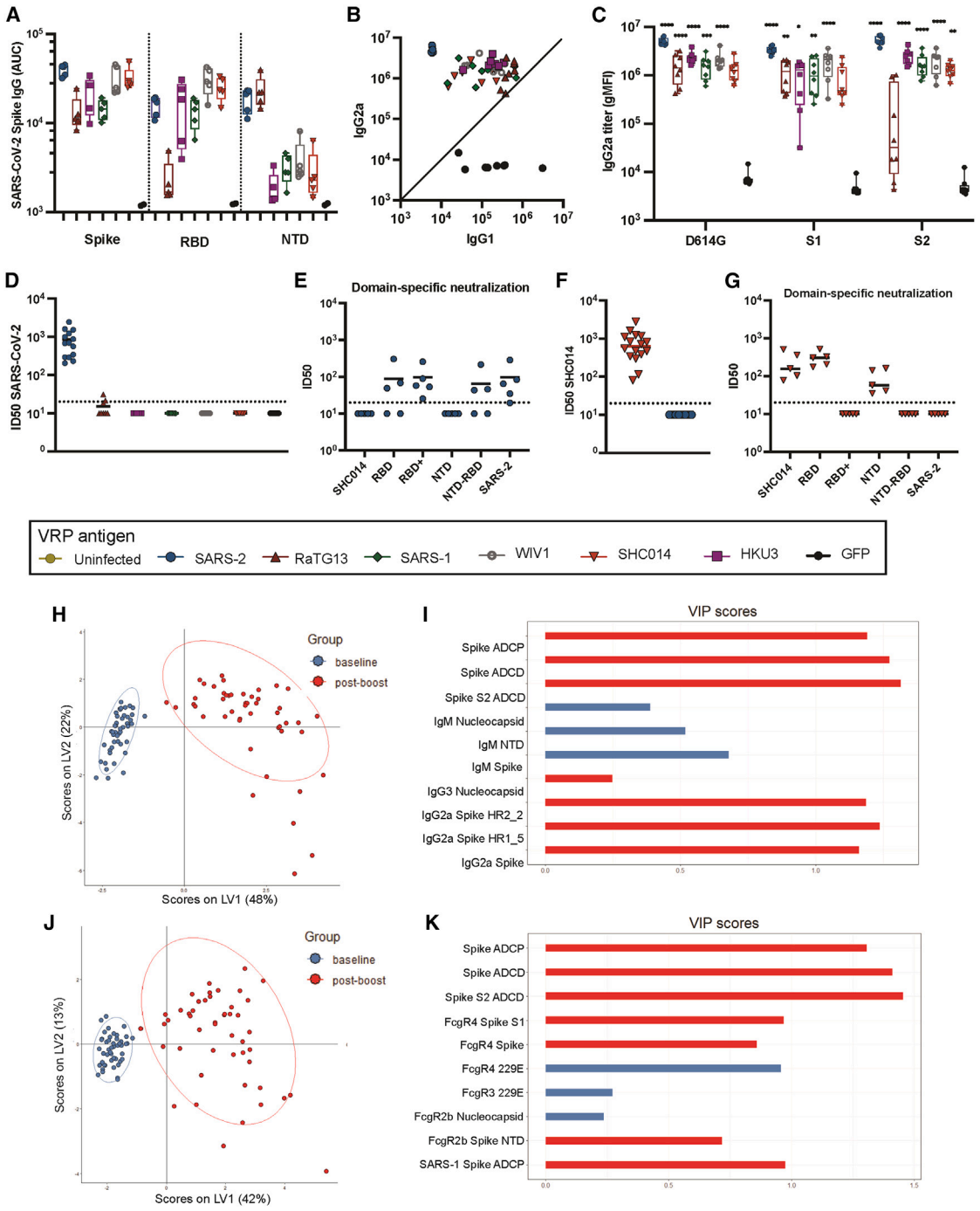

Figure 5. Characterizing the antibody response through systems serology and functional assays

(A) SARS-CoV-2 spike (left), receptor binding domain (middle), and N-terminal domain (right) binding IgG quantified by ELISA. Titers calculated via AUC.

(B) SARS-CoV-2 spike binding IgG2a titers plotted against IgG1 titers. Titer calculated by geometric mean fluorescence intensity (gMFI).

(C) SARS-CoV-2 spike (left), S1 (middle), and S2 (right) binding IgG2a titer calculated by gMFI via Luminex bead assay.

(D) SARS-CoV-2 neutralization IC_{50} values calculated as the serum dilution that achieved 50% neutralization in a live-virus neutralization assay.

(E) Domain-specific IC_{50} values measured by live-virus neutralization assay against different SARS-CoV-2 spike domains on a heterologous virus backbone (SHC014).

(F) SHC014 neutralization IC_{50} values of serum from vaccinated animals.

(G) Domain-specific IC_{50} values measured by live-virus neutralization assay against different SARS-CoV-2 spike domains on the SHC014 backbone. IC_{50} for samples that fell below the limit of detection (dotted line) were set to 10.

(legend continued on next page)

neutralizing antibodies against the SARS-CoV-2 NTD or S2 (Figure 5E). Using this assay, we also found that VRP SHC014 spike-elicited neutralizing antibodies preferentially targeted the NTD and RBD+ regions, as shown by a complete loss of neutralization when either the RBD+ or NTD-RBD (amino acids 13–528) (Figure 5G) were exchanged. Together, neutralizing antibody responses elicited by VRP spike vaccines are highly type and domain specific, supporting the hypothesis that cross-neutralizing antibodies do not drive VRP cross-protection between sarbecoviruses.

Given the lack of cross-neutralizing antibodies despite clear cross-protection, we further employed systems serology to characterize the overall humoral architecture in response to our VRP candidates[32,40,51] (Figure S4). An initial multivariate discriminate analysis (partial least squares discriminant analysis [PLS-DA]) evaluated whether the serological characteristics could differentiate between baseline and post-boost groups as well as predict the minimal distinguishing features that could differentiate between groups. Features were selected via least absolute shrinkage and selection operator (LASSO) as previously described,[51] classified using a fold-specific support vector machine (SVM), and variables were identified and classified via PLS-DA visualization. To obtain optimal resolution on feature identification and validate our findings, we ran two models that included functional assays with (1) Ig subclass (Figure 5H) and (2) FcR affinity (Figure 5J). Validations via randomization confirmed that the LASSO/SVM could significantly differentiate selected features from randomly selected features and permutations (Figure S5). The PLS-DA demonstrated a strong clustering of challenged animals away from baseline for both Ig subclass (Figure 5H) and FcR-binding (Figure 5J) antibodies. Through calculating the variable importance in protection (VIP) scores for both Fab and FcR binding profiles,[51] we found that IgG2a binding to both full-length spike and S2 subdomains (Figure 5I) as well as FcgR4-binding antibodies toward full-length spike and the S1 domain (Figure 5K) most significantly separated the baseline from post-boost. Interestingly, Fc-mediated, non-neutralizing functions such as antibody-dependent complement deposition (ADCD) and ADCP were also among the highest ranked in both models. Similar to our previous analysis, PLS-DA identified that humoral recognition of both S1 and S2 subregions was driving the phenotype and not simply RBD-responsive antibodies, which bear the majority of neutralizing activity.

To more closely delineate protective signatures stimulated by the VRP spike vaccines, we performed a series of cross-correlative analyses (Figure S6). To summarize the correlation matrices and identify trends, we highlighted associations with strong, significant correlations (0.7–1, $p < 0.05$) from each VRP spike vaccine, focusing on IgG2a, functional assays, and Fc-gamma receptors FcgR3/R4 (Figure 6A). Strikingly, while numerous S1 and S2 correlates were identified, there was little overlap between the two. Recognition of S2 by various VRP spike sera was tied to Fc-effector-mediated functions, while S1 demonstrated strong correlations with FcgR4 but was not statistically tied to effector functions (Figures 6A and 6B). Using a peptide scanning array that spanned the majority of S2, we identified that heptad repeat region 2 (HR2), the fusion peptide (FP), and the stalk subregions drove much of the IgG2a recognition. Notably, we found that full spike, S2, and S2 subdomain-specific IgG2a correlated with the phagocytic functional assays (antibody-dependent neutrophil phagocytosis [ADNP]/ADCP) in the more distant heterologous VRP spike vaccines (HKU3, SARS-CoV, WIV1, SHC014). We also found that the VRP SARS-CoV-2 and the more protective spike vaccines (HKU3, RaTG13) IgG2a correlated with ADCD (Figure 6A). Generally, FcR affinity exhibited clade dependence. FcgR4 was most stimulated by antibodies raised to the clade 1b and 2 VRP spike sera (SARS-CoV-2, RaTG13, and HKU3), and less so by those raised to clade 1a VRP spike sera (SARS, SHC014, and WIV1) (Figure 6B). Consequently, we evaluated the capacity for the VRP spike serum to stimulate ADCP and ADNP against the SARS-CoV-2 full spike as previously described.[32,52] Overall, although not clade dependent, we found notable and significant increases in ADNP (Figure 6C), ADCP (Figure 6D), and ADCD (Figure 6E) against the SARS-CoV-2 full spike in VRP spike vaccine sera.

Our data demonstrate that VRP spike-specific, non-neutralizing antibodies stimulate FcR effector functions that are mechanistically linked to FcgR4 binding IgG2a. Additional heatmap analysis of the heterologous VRP spike sera (Figure S7) indicated that not only did IgG2a cluster very well with itself but the heptad repeat regions (HR1, HR2) and stalk subdomains of spike also exhibited the greatest strength of binding (Figure S7A). When evaluating subclass binding within S2, a peptide scanning array also indicated that VRP vaccination induced IgG2a with strong recognition of HR1, HR2, FP, and stalk subdomains of S2 relative to controls (Figure S7B).

Since VRP HKU3 and RaTG13 spike vaccines induced high protection against heterologous SARS-CoV-2 challenge, we investigated a correlation between domain-specific antibody binding and disease severity. The magnitude of VRP HKU3 spike serum IgG2a binding the HR1 shared a strong, significant

(H) A scores plot representing the baseline (blue) and post-boost (red) vaccine immunoglobulin and functional profile distribution for all vaccinated animals tested, clustered via partial least squares discriminant analysis (PLSDA).

(I) VIP score of most influential features, representing the total distance from the center of the scores plot, as determined by PLSDA of immunoglobulin and functional profiles.

(J) A scores plot representing the baseline (blue) and post-boost (red) vaccine Fc receptor stimulation and functional profile distribution for all vaccinated animals tested, clustered via PLSDA.

(K) VIP score of most influential features, representing the total distance from the center of the scores plot, as determined by PLSDA of Fc receptor stimulation and functional profiles. Significance calculations: antibody titers, one-way ANOVA corrected for multiple comparisons using Dunnett's multiple comparisons test, and Dunnett's T3 test when total samples <50. *$p < 0.05$, **$p < 0.01$, ***$p < 0.001$, ****$p < 0.0001$. PLSDA was done on R using the systemsseRology pipeline available on GitHub (https://github.com/LoosC/systemsseRology). Machine learning tools (for the analysis of systems serology data) are also available. Each assay contained pre-immune and post-vaccination sera, as well as PBS controls to account for batch effects.

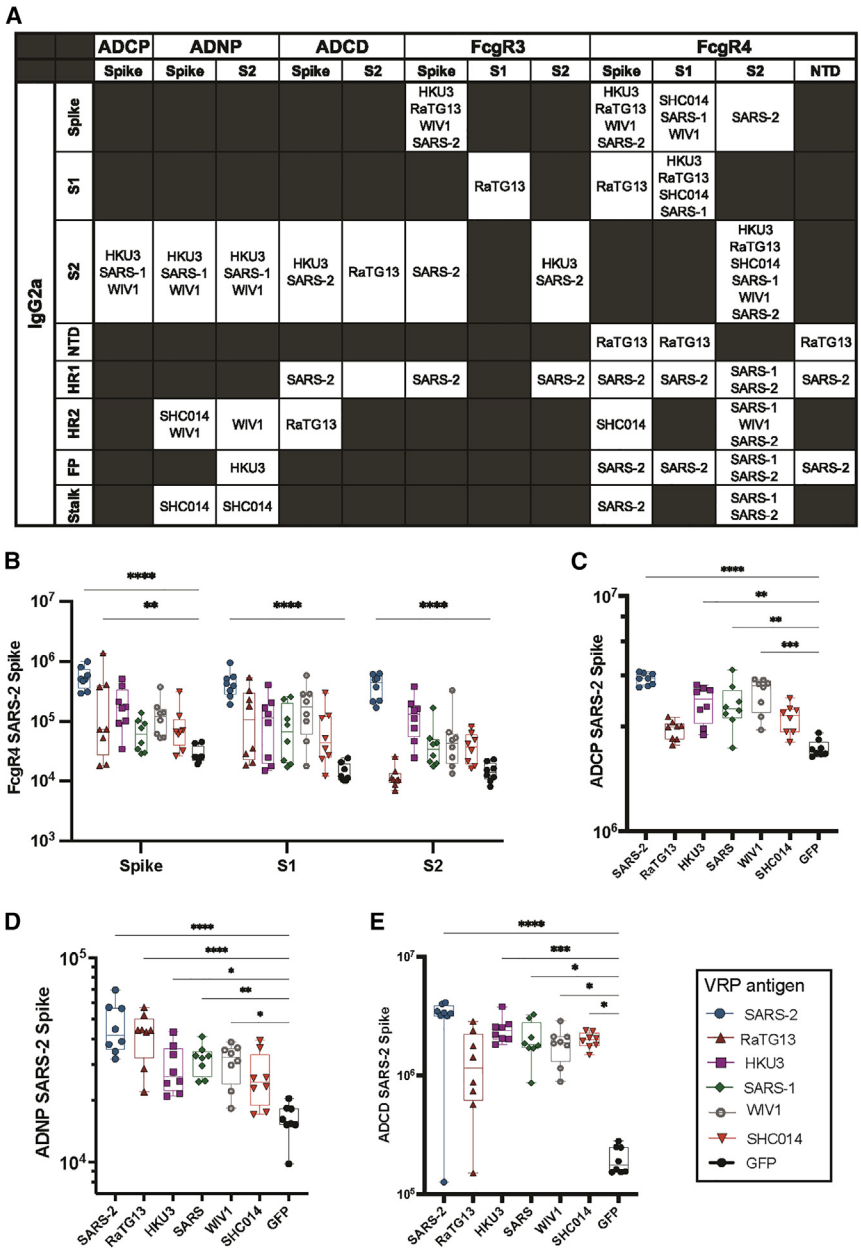

Figure 6. Correlation between FcR function and antibody cross-simulation

(A) Pearson's correlation matrices were constructed of the systems serology assays for each VRP vaccination group (supplemental data). VRP vaccine groups with strong correlations (0.7–1) between two assay results are listed in the table.

(B) FcgR4 stimulation against the SARS-2 spike (left), S1 (middle), and S2 (right).

(C) Phagocytic score of antibody-dependent neutrophil phagocytosis (ADNP).

(D and E) (D) Phagocytic score of antibody-dependent cellular phagocytosis (ADCP) and (E) antibody-dependent complement deposition (ADCD) score (gMFI). Correlations between Fab, FcR, and functional assays were done using GraphPad Prism using Spearman's coefficients. Statistical significance, as defined by $p < 0.05$, was corrected for multiple comparisons using Benjamini-Hochberg correction. Each assay contained pre-immune and post-vaccination sera, as well as PBS controls to account for batch effects. The univariate significance of antibody function (B–E) was calculated via one-way ANOVA comparing each spike-vaccinated group with the GFP control. Testing was corrected for multiple comparisons using Dunnett's multiple comparisons test, and Dunnett's T3 test when total samples <50. Significance reported as *$p < 0.05$, **$p < 0.01$, ***$p < 0.001$, ****$p < 0.0001$.

correlation (Pearson's $r = 0.92$, $p < 0.05$, $n = 4$) with protection from disease represented by body weight maintenance. Likewise, VRP RaTG13 sera S2 binding also showed a very significant correlation (Pearson's $r = 0.91$, $p < 0.05$, $n = 4$) with protection. We found significant correlations between protection and antibody binding in most S2 subdomains for WIV1 but, in contrast to most other vaccine groups, failed to detect correlations between protection and functional assays such as ADCD and ADCP for WIV1. We also found that *in vivo* protection elicited by other VRP spike vaccines was linked to S2 but not single domains. Notably the SHC014 VRP spike vaccine was also closely linked to the NTD (Figure S7C). These data suggest that the sum of smaller fractions of cross-reactive antibody responses may also affect protection, in addition to the capacity of the binding antibodies to stimulate protective FcR effector responses. Within S2, the HR2 subdomain is 100% conserved between the sarbecovirus spikes tested. The HR1 subdomain of RaTG13 and HKU3 is also 100% and 98.7% identical to the SARS-CoV-2 HR1 subdomain, respectively. In contrast, the HR1 subdomains of the clade 1a sarbecovirus spikes, which showed less protection, share 88.3%–89.6% identity with the SARS-CoV-2 spike HR1 (Figure S7D). Sequence conservation in linear epitopes of S2, especially HR1, in addition to cellular functional stimulation likely drove the cross-protective, non-neutralizing antibody response elicited by VRP-vectored sarbecovirus spikes.

VRP spike vaccinations induce antibody-mediated protection via Fc effector mechanism

Given indications of non-neutralizing, antibody-dependent cellular function by serological assays, prophylactic passive transfer experiments were used to evaluate the role of antiserum in cross-protection from clinical disease. Serum from VRP spike (SARS-CoV-2, SARS-CoV, HKU3, and GFP)-vaccinated mice was pooled for each group and administered intraperitoneally into naive mice. Twenty-four hours later, the mice were challenged with a lethal 10^4 PFU MA10 dose. Importantly, SARS-CoV-2 and

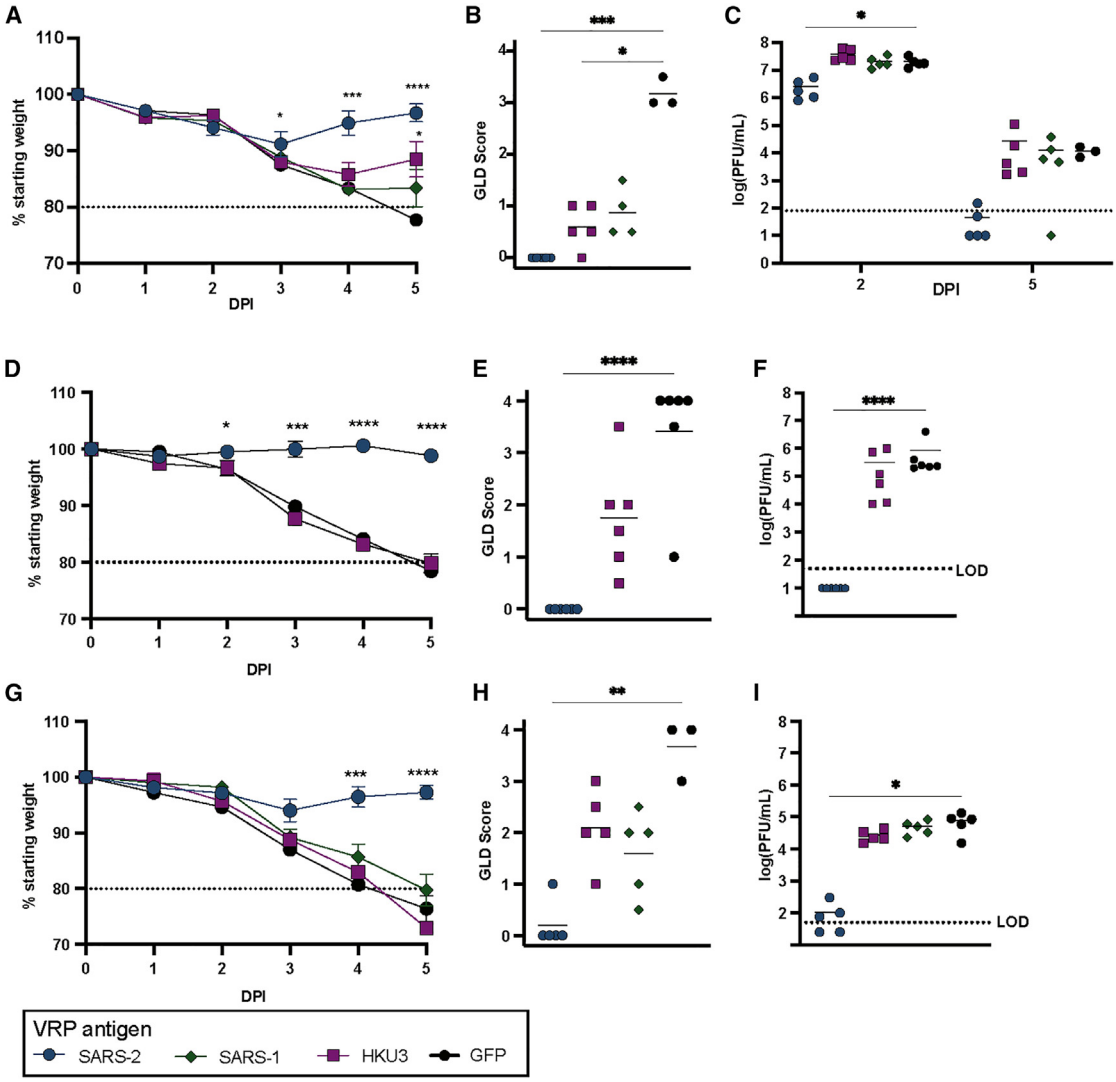

Figure 7. Non-neutralizing antibodies mediate protection *in vivo* through Fc function

(A–C) (A) Body weights, (B) GLD scores day 5 post-infection, and (C) SARS-2 lung titer in naive mice after passive transfer of serum from vaccinated animals followed by intranasal infection of 10^4 PFU SARS-2.

(H–J) (H) Body weights, (I) GLD scores day 5 post-infection, and (J) SARS-2 lung titer of young Fc receptor knockout BALB/c mice that were vaccinated with a sarbecovirus spike protein prior to infection with 10^4 PFU SARS-2 intranasally.

(D–F) (D) Body weights, (E) GLD scores day 5 post-infection, and (F) SARS-CoV-2 lung titer of young Fc receptor knockout BALB/c mice that received prophylactic administration of serum from vaccinated wild-type BALB/c mice prior to infection with 10^3 PFU SARS-CoV-2 intranasally. All FcR knockout mice were obtained from Taconic (n = 5–6 per sacrifice day). Wild-type mice were tested from both Envigo (consistent with previous reported work) and Taconic (strain-specific match) to account for strain-specific differences. Taconic n = 5 per day reported. Body weights reported as percentage of starting weight where horizontal line indicates 20% body weight lost and animal care humane endpoint. Titer samples that fell below the limit of detection (dotted line) were set to 25 PFU/mL. Mean data points, arithmetic mean; error bars, standard error from the mean. Significance calculations: weight loss, two-way ANOVA; weight loss in cases of mortality, mixed-effects analysis; virus titer, one-way ANOVA; GLD scoring, Brown-Forsythe and Welch's ANOVA; all corrections, Dunnett's, T3 when total samples <50. *p < 0.05, **p < 0.01, ***p < 0.001, ****p < 0.0001.

HKU3 VRP serum recipients experienced significant reductions in weight loss by day 5 post-infection, while the SARS-CoV VRP serum recipients developed more severe weight loss that was not significantly reduced (Figure 7A). We also observed significant reductions in GLD in all groups, demonstrating that passive transfer of antibodies mitigated severe/lethal disease (Figure 7B). This was in contrast with viral loads, which were exclusively mitigated by the VRP SARS-CoV-2 spike vaccine serum (Figure 7C), providing further support to the hypothesis that neutralizing antibodies play a substantial role in limiting viral replication and disease, whereas non-neutralizing antibodies primarily mitigate disease pathology. Collectively, these data suggest that there is a clear role for non-neutralizing antibodies in vaccine cross-protection against SARS-CoV-2.

To further probe the mechanism of VRP spike cross-protection, we vaccinated FcR-deficient BALB/c mice before lethal challenge with MA10. We found that, when Fc effector function was effectively eliminated, protection against SARS-CoV-2 disease by vaccination with VRP HKU3 spike was lost (Figures 7D–7F). Both rapid/sustained weight loss (Figure 7D) and GLD (Figure 7E) were evident in the FcR KO mice immunized with VRP HKU3 spike and, unlike WT mice, were statistically indistinguishable from GFP-vaccinated mice. However, FcR-deficient mice vaccinated with VRP SARS-CoV-2 spike were still protected from clinical disease and virus replication, again consistent with a strong homologous neutralizing antibody response (Figure 7F). This indicates that cross-protection is mechanistically linked to FcR-mediated responses despite a potent homologous protective profile. We then conducted a prophylactic passive transfer experiment in FcR-deficient BALB/c mice prior to lethal challenge with MA10. VRP SARS-CoV-2 spike homologous sera still protected against severe disease in the absence of FcR effector function, as shown by weight loss (Figure 7G) and GLD scores (Figure 7H). Animals that received VRP SARS-CoV-2 spike sera also significantly suppressed virus replication, again supporting a strongly protective role for homologous neutralizing antibody response (Figure 7I). However, the heterologous SARS-CoV and HKU3 spike VRP sera failed to protect in FcR-deficient mice (Figures 7G–7I). Compared with wild-type mice, weight loss and GLD increased in FcR-deficient mice, with no decrease in virus titer. FcR-deficient mice that received heterologous VRP spike sera also surpassed 20% weight loss, indicative of lethal disease. Thus, while strain-specific antibodies capable of neutralization can protect from disease, cross-protection is mechanistically linked to non-neutralizing, FcR-mediated responses.

DISCUSSION

The COVID-19 pandemic resulted in massive human suffering and global economic upheavals. The continued spread of SARS-CoV-2 VOC coupled with large numbers of zoonotic reservoir strains poised for cross-species movement indicate that robust countermeasures that elicit broad, cross-protective immune responses offer a strategic approach for controlling sarbecovirus epidemics. Although potent neutralizing antibodies are a benchmark for COVID-19 vaccine efficacy, recent work found that SARS-CoV-2 S2P mRNA vaccines elicited limited cross-neutralizing antibody titers against heterologous sarbecoviruses, including the SARS-CoV-2 Omicron VOC.[13,53,54] Moreover, several studies have suggested non-neutralizing antibodies function in protection against SARS-CoV-2 disease, both long and short term,[30,31,34,55,56] highlighting a critical need for identification of pan-sarbecovirus protective immune correlates. As alphavirus replicons that induce mucosal, humoral, and cellular immune responses against respiratory pathogens,[57,58] they provide innovative models for understanding cross-immune mechanisms.[59–61] In the present study, we found that non-neutralizing antibodies can contribute to broad cross-vaccine protective immunity across clade 1a, 1b, and clade 2 sarbecoviruses, with as little as 75% amino acid identity between spike protein sequences. These studies highlight an important protective role for non-neutralizing antibodies, especially in cases of heterologous virus infection across distant sarbecoviruses, via antibody interactions with FcR effector functions as a driver of protective immunity.[31]

Highly potent mRNA vaccines target neutralizing antibody responses to the S1 RBD domain[62,63] and potent neutralizing antibodies targeting one or more epitopes in the RBD,[23] NTD,[64] or S2[65,66] have been identified in spike. Consistent with established work, we identified a neutralizing antibody response stimulated by the VRP platform but failed to detect protective levels of cross-neutralizing antibodies even though conserved regions of the spike have been identified.[23,29,62] Our data also suggest that different sarbecoviruses may focus neutralizing antibody responses to different sites within S1, potentially complicating universal vaccine platforms focused exclusively on the RBD, especially when applied to outbred populations such as the human population.[67,68]

Similar cross-protective phenotypes identified in our study have previously been identified but mediated by CoV nucleocapsid-based vaccines that stimulate T cells following SARS-CoV and MERS-CoV challenge.[69] Our data do not explicitly rule out a contribution of T cells in mediating protection after VRP vaccination. However, this study implicates non-neutralizing antibody functions as strong drivers of cross-protection. We also found no evidence of antibody-dependent enhancement by the non-neutralizing antibodies. Virus replication was never significantly higher than the negative control vaccine groups *in vivo*, nor did we detect enhanced replication in our *in vitro* neutralization assays. Further, disease was not enhanced by prophylactic antibody transfers in either wild-type or FcR-deficient mice, indicating that, in the absence of FcR function, the non-neutralizing antibodies will not enhance disease.

In this model, cross-protection was highly clade dependent, suggesting that specific domain conservation rather than overall sequence homology drives the development of protective antibodies in our model. Additionally, we found that VRP SARS-CoV-2 spike vaccination protected from severe disease after heterologous challenge, aligning with current data regarding spike-based vaccine efficacy against SARS-CoV-2 variants in the human population where currently approved vaccines may not prevent variant infection in all cases but significantly reduce disease severity and death.[70–73] However, contemporary human CoV spike vaccines did not protect against SARS-CoV-2. Contrary to some earlier correlative studies,[17,74–77] these differences may reflect repeat group 1A/2B human β-CoV infections, which might result in more cross-protective humoral responses, highlighting an area of future investigation.

Both homologous and heterologous protection were less robust in aged animals.[37,47] Notably, age-related waning of FcR effector functions is thought to affect both vaccine efficacy and infection response,[78–80] including dysregulated neutrophil responses after pulmonary infection[80] and impaired overall effector cell function.[78,79,81,82] Thus, as a function of increasing virus challenge dose in aged animals, increased VRP sarbecovirus spike vaccine failure is consistent with reduced FcR-mediated protection, a prospect that will need to be carefully investigated in future vaccine studies focused on more vulnerable elderly populations.

Not only are VRPs a valuable experimental platform for studying cross-protective CoV immunity, especially regarding non-neutralizing antibody responses, they also highlight many areas for further investigation. The same susceptibility loci appear to regulate sarbecovirus pathogenesis in mice and humans,[49] and the mouse model reproduces key aspects of acute and chronic SARS-CoV-2-induced disease.[39,42] Furthermore, mouse models of SARS-CoV-2 disease have proven to be robust platforms for predicting SARS-CoV-2 vaccine performance in humans,[49,83–85] and the alphavirus replicon strategy has shown utility as a vaccine platform.[86–89] Systems serology responses following alphavirus vaccination in humans have not been reported, including any reporting on non-neutralizing antibody functional activity. This study has clearly implicated FcR-mediated protection following alphavirus VRP vaccination in mice as well as directly correlated the FcR mechanism of cross-protection to disease outcome. However, our data were drawn from a limited sample size for correlation to disease, prompting a need for further mechanistic investigation into the immune cell types that modulate interclade sarbecovirus non-neutralizing antibody and FcR-mediated cross-protection. Still, detailed systems serology studies have also suggested a robust correlative role for FcR-mediated protection after vaccination and the durability of protection compared with prior infection in SARS-CoV-2, human immunodeficiency virus, influenza virus, and dengue virus vaccination and prior infection.[40,90,91] Our work indicates that FcR mechanisms are primary drivers of protection in this model, and further antibody manipulations, including analysis of F(ab)2 fragments or LALAPG mutations that disrupt FcR and complement mediated antibody effector functions,[92] may further define the cell types involved.

The results identified here may be relevant to understanding the mechanisms that promote vaccine-induced SARS-CoV-2 immunity in humans. However, most vaccine designs have not been tailored to maximize protective FcR effector functions despite clear animal model results demonstrating that activation of distinct FcγR-mediated pathways significantly improves antibody-mediated protection and sustains robust immune responses.[34,91,93,94] Although these studies implicate S2, but not RBD, as a major target of antibody responses, the exact antibodies and epitopes that contribute to cross-protection via FcR-mediated activities remain unclear. This information would guide development of future pan-CoV therapeutics and vaccines. This is especially relevant in VRP HKU3 cross-protection, where identification of novel spike epitopes may supplement broad cross-protection through FcR effector responses. It will also be essential to determine whether these results extend beyond standard inbred mouse strains by testing their impact in outbred populations, such as the Collaborative Cross,[95,96] or other models of SARS-CoV-2-induced disease such as non-human primates.

As SARS-CoV-2 is the second sarbecovirus to emerge in the twenty-first century, other CoVs will likely arise in the future, including those with similar or different spike sequences to those examined in this study (e.g., SHC014 and WIV1)[4] and others (e.g., swine acute diarrhea syndrome [SADS] CoV).[97] Therefore, the inclusion of non-neutralizing, cross-protective epitopes informed by the results of our and future studies may shift vaccine development toward a more comprehensive, cross-protective formulation that prevents life-threatening sarbecovirus disease and provide new insights for vaccine design against other highly heterogeneous RNA virus families, including Coronaviridae.

Limitations of the study

Our study was composed primarily of *in vivo* challenge studies and the characterization of the immune response outcomes in BALB/c mice. While the MA10 model has been useful for evaluating the efficacy of SARS-CoV-2 vaccines and therapeutics,[12,43,98,99] and recent pre-publication work details complementary data of FcR-dependent CoV protection to our model,[100] the Fc receptor functions and functional cellular mechanisms of immune protection differ between mice and humans in addition to the affinity of those cells and receptors for antibody subclasses.[35] Moving forward, analyses in rodent genetic reference models of outbred populations[49,96] and humanized FcR mice would enable refined conclusions regarding the role of FcR function in cross-sarbecovirus protection, and serological studies from human donors may provide more context to the cross-protective mechanisms in the human population. We recognize the possibility that differences in host immune cell types may also contribute to non-neutralizing FcR-mediated pan-sarbecovirus protection, requiring additional experimentation. Importantly, our approach can be applied to multiple vaccine designs and microbial pathogens, leading to improvements in universal vaccines.

STAR★METHODS

Detailed methods are provided in the online version of this paper and include the following:

- KEY RESOURCES TABLE
- RESOURCE AVAILABILITY
  - Lead contact
  - Materials availability
  - Data and code availability
- EXPERIMENTAL MODEL AND SUBJECT DETAILS
  - Biosafety and institutional approval
  - Cell lines
  - Animal models
  - Viruses
- METHOD DETAILS
  - VEE VRP3526 vaccine preparation
  - Mice, vaccination, and infection
  - Mouse tissue collection and analysis
  - Neutralization assays
  - Systems serology
  - Enzyme-linked immunosorbent assay
- QUANTIFICATION AND STATISTICAL ANALYSIS
  - Systems serology
  - Other statistical testing

SUPPLEMENTAL INFORMATION

Supplemental information can be found online at https://doi.org/10.1016/j.celrep.2023.112326.

ACKNOWLEDGMENTS

G.A. (Systems Serology Lab at Ragon) is supported by Mark and Lisa Schwartz, Terry and Susan Ragon, and the SAMANA Kay MGH Research Scholars award. The Systems Serology Lab also receives funding from the Massachusetts Consortium on Pathogen Readiness (MassCPR), the Gates Global Health Vaccine Accelerator Platform, and NIH (3R37AI080289-11S1, R01AI146785, U19AI42790-01, U19AI135995-02, U19AI42790-01, P01AI165072, U01CA260476 – 01, CIVIC75N93019C00052). V.K.B. receives funding from NIH grant K01OD026529. R.S.B. and M.T.H. are supported by NIH grant P01AI158571. R.S.B. receives funding from NIH/NCI North Carolina Seronet Center for Excellence grant U54 CA260543. L.E.A. was supported in part by NIH 2T32AI007419-26 Molecular Biology of Viral Diseases Predoctoral Training grant. This project was also supported in part by the North Carolina Policy Collaboratory at the University of North Carolina at Chapel Hill with funding from the North Carolina Coronavirus Relief Fund established and appropriated by the North Carolina General Assembly. We would also like to thank Sharon Taft-Benz for valuable input coordinating, directing, and managing studies in ABSL3 facilities.

AUTHOR CONTRIBUTIONS

Conceptualization, R.S.B., M.T.H., and L.E.A.; methodology, R.S.B., M.T.H., V.K.B., S.A.M., L.E.A., S.R.L., K.H.D., R.P.M., G.A., and L.P.; software, R.P.M. and G.A.; validation, L.E.A.; formal analysis, L.E.A., R.P.M., and G.A.; investigation, L.E.A., S.R.L., K.H.D., A.W., K.L.G., J.F.L., E.A.M., J.M.P., A.S., S.S., I.N.C., J.S.M., R.P.M., H.L.B., S.S.M., V.K.B., and M.T.H.; resources, K.L.G., M.R.Z., J.S.H., and B.K.H.; data curation, L.E.A., R.P.M., and I.N.C.; writing – original draft, L.E.A., R.P.M., M.T.H., and R.S.B.; writing – review & editing, L.E.A., S.R.L., K.H.D., J.F.L., E.A.M., R.P.M., S.A.M., V.K.B., M.T.H., and R.S.B.; visualization, L.E.A., R.P.M., and V.K.B.; supervision, G.A., V.K.B., M.T.H., and R.S.B.; project administration, L.E.A., M.T.H., and R.S.B.; funding acquisition, L.E.A., G.A., M.T.H., and R.S.B.

DECLARATION OF INTERESTS

G.A. is a founder/equity holder in Seroymx Systems and Leyden Labs. G.A. has served as a scientific advisor for Sanofi Vaccines. G.A. has collaborative agreements with GSK, Merck, Abbvie, Sanofi, Medicago, BioNtech, Moderna, BMS, Novavax, SK Biosciences, Gilead, and Sanaria. R.S.B. has served as a consultant for Takeda and Sanofi Pasteur vaccines and is a member of the Scientific Advisory Board of VaxArt and Invivyd. R.S.B. has unrelated collaborations with J&J, Gilead, Ridgeback Biosciences, and Moderna.

Received: October 18, 2022
Revised: December 21, 2022
Accepted: March 17, 2023

REFERENCES

1. Rota, P.A., Oberste, M.S., Monroe, S.S., Nix, W.A., Campagnoli, R., Icenogle, J.P., Peñaranda, S., Bankamp, B., Maher, K., Chen, M.-H., et al. (2003). Characterization of a novel coronavirus associated with severe acute respiratory syndrome. Science *300*, 1394–1399. https://doi.org/10.1126/science.1085952.
2. Zhou, P., Yang, X.-L., Wang, X.-G., Hu, B., Zhang, L., Zhang, W., Si, H.-R., Zhu, Y., Li, B., Huang, C.-L., et al. (2020). A pneumonia outbreak associated with a new coronavirus of probable bat origin. Nature *579*, 270–273. https://doi.org/10.1038/s41586-020-2012-7.
3. Menachery, V.D., Yount, B.L., Sims, A.C., Debbink, K., Agnihothram, S.S., Gralinski, L.E., Graham, R.L., Scobey, T., Plante, J.A., Royal, S.R., et al. (2016). SARS-like WIV1-CoV poised for human emergence. Proc. Natl. Acad. Sci. USA *113*, 3048–3053. https://doi.org/10.1073/pnas.1517719113.
4. Menachery, V.D., Yount, B.L., Debbink, K., Agnihothram, S., Gralinski, L.E., Plante, J.A., Graham, R.L., Scobey, T., Ge, X.-Y., Donaldson, E.F., et al. (2015). A SARS-like cluster of circulating bat coronaviruses shows potential for human emergence. Nat. Med. *21*, 1508–1513. https://doi.org/10.1038/nm.3985.
5. Lau, S.K.P., Woo, P.C.Y., Li, K.S.M., Huang, Y., Tsoi, H.-W., Wong, B.H.L., Wong, S.S.Y., Leung, S.-Y., Chan, K.-H., and Yuen, K.-Y. (2005). Severe acute respiratory syndrome coronavirus-like virus in Chinese horseshoe bats. Proc. Natl. Acad. Sci. USA *102*, 14040–14045. https://doi.org/10.1073/pnas.0506735102.
6. Li, W., Shi, Z., Yu, M., Ren, W., Smith, C., Epstein, J.H., Wang, H., Crameri, G., Hu, Z., Zhang, H., et al. (2005). Bats are natural reservoirs of SARS-like coronaviruses. Science *310*, 676–679. https://doi.org/10.1126/science.1118391.
7. Temmam, S., Vongphayloth, K., Baquero, E., Munier, S., Bonomi, M., Regnault, B., Douangboubpha, B., Karami, Y., Chrétien, D., Sanamxay, D., et al. (2022). Bat coronaviruses related to SARS-CoV-2 and infectious for human cells. Nature *604*, 330–336. https://doi.org/10.1038/s41586-022-04532-4.
8. Arya, R., Kumari, S., Pandey, B., Mistry, H., Bihani, S.C., Das, A., Prashar, V., Gupta, G.D., Panicker, L., and Kumar, M. (2021). Structural insights into SARS-CoV-2 proteins. J. Mol. Biol. *433*, 166725. https://doi.org/10.1016/j.jmb.2020.11.024.
9. Adams, L.E., Dinnon, K.H., Hou, Y.J., Sheahan, T.P., Heise, M.T., and Baric, R.S. (2021). Critical ACE2 determinants of SARS-CoV-2 and group 2B coronavirus infection and replication. mBio *12*, e03149-20. https://doi.org/10.1128/mBio.03149-20.
10. Wan, Y., Shang, J., Graham, R., Baric, R.S., and Li, F. (2020). Receptor recognition by the novel coronavirus from Wuhan: an analysis based on decade-long structural studies of SARS coronavirus. J. Virol. *94*, e00127-20. https://doi.org/10.1128/JVI.00127-20.
11. Becker, M.M., Graham, R.L., Donaldson, E.F., Rockx, B., Sims, A.C., Sheahan, T., Pickles, R.J., Corti, D., Johnston, R.E., Baric, R.S., et al. (2008). Synthetic recombinant bat SARS-like coronavirus is infectious in cultured cells and in mice. Proc. Natl. Acad. Sci. USA *105*, 19944–19949. https://doi.org/10.1073/pnas.0808116105.
12. Corbett, K.S., Edwards, D.K., Leist, S.R., Abiona, O.M., Boyoglu-Barnum, S., Gillespie, R.A., Himansu, S., Schäfer, A., Ziwawo, C.T., DiPiazza, A.T., et al. (2020). SARS-CoV-2 mRNA vaccine design enabled by prototype pathogen preparedness. Nature *586*, 567–571. https://doi.org/10.1038/s41586-020-2622-0.
13. Martinez, D.R., Schäfer, A., Leist, S.R., De la Cruz, G., West, A., Atochina-Vasserman, E.N., Lindesmith, L.C., Pardi, N., Parks, R., Barr, M., et al. (2021). Chimeric spike mRNA vaccines protect against Sarbecovirus challenge in mice. Science *373*, 991–998. https://doi.org/10.1126/science.abi4506.
14. Olotu, F.A., Omolabi, K.F., and Soliman, M.E.S. (2020). Leaving no stone unturned: allosteric targeting of SARS-CoV-2 spike protein at putative druggable sites disrupts human angiotensin-converting enzyme interactions at the receptor binding domain. Inform. Med. Unlocked *21*, 100451. https://doi.org/10.1016/j.imu.2020.100451.
15. Díaz-Salinas, M.A., Li, Q., Ejemel, M., Yurkovetskiy, L., Luban, J., Shen, K., Wang, Y., and Munro, J.B. (2022). Conformational dynamics and allosteric modulation of the SARS-CoV-2 spike. Elife *11*, e75433. https://doi.org/10.7554/eLife.75433.
16. Hassan, A.O., Case, J.B., Winkler, E.S., Thackray, L.B., Kafai, N.M., Bailey, A.L., McCune, B.T., Fox, J.M., Chen, R.E., Alsoussi, W.B., et al. (2020). A SARS-CoV-2 infection model in mice demonstrates protection by neutralizing antibodies. Cell *182*, 744–753.e4. https://doi.org/10.1016/j.cell.2020.06.011.
17. Mateus, J., Grifoni, A., Tarke, A., Sidney, J., Ramirez, S.I., Dan, J.M., Burger, Z.C., Rawlings, S.A., Smith, D.M., Phillips, E., et al. (2020). Selective and cross-reactive SARS-CoV-2 T cell epitopes in unexposed humans. Science *370*, 89–94. https://doi.org/10.1126/science.abd3871.

18. Zhu, Y., Yu, D., Han, Y., Yan, H., Chong, H., Ren, L., Wang, J., Li, T., and He, Y. (2020). Cross-reactive neutralization of SARS-CoV-2 by serum antibodies from recovered SARS patients and immunized animals. Sci. Adv. *6*, eabc9999. https://doi.org/10.1126/sciadv.abc9999.

19. Xie, X., Liu, Y., Liu, J., Zhang, X., Zou, J., Fontes-Garfias, C.R., Xia, H., Swanson, K.A., Cutler, M., Cooper, D., et al. (2021). Neutralization of SARS-CoV-2 spike 69/70 deletion, E484K and N501Y variants by BNT162b2 vaccine-elicited sera. Nat. Med. *27*, 620–621. https://doi.org/10.1038/s41591-021-01270-4.

20. Rappazzo, C.G., Tse, L.V., Kaku, C.I., Wrapp, D., Sakharkar, M., Huang, D., Deveau, L.M., Yockachonis, T.J., Herbert, A.S., Battles, M.B., et al. (2021). Broad and potent activity against SARS-like viruses by an engineered human monoclonal antibody. Science *371*, 823–829. https://doi.org/10.1126/science.abf4830.

21. Nelde, A., Bilich, T., Heitmann, J.S., Maringer, Y., Salih, H.R., Roerden, M., Lübke, M., Bauer, J., Rieth, J., Wacker, M., et al. (2021). SARS-CoV-2 T-Cell Epitopes Define Heterologous and COVID-19-Induced T-Cell Recognition. Nat. Immunol. *22*, 74–85. https://doi.org/10.21203/rs.3.rs-35331/v1.

22. Liu, L., Wang, P., Nair, M.S., Yu, J., Rapp, M., Wang, Q., Luo, Y., Chan, J.F.-W., Sahi, V., Figueroa, A., et al. (2020). Potent neutralizing antibodies against multiple epitopes on SARS-CoV-2 spike. Nature *584*, 450–456. https://doi.org/10.1038/s41586-020-2571-7.

23. Pinto, D., Park, Y.-J., Beltramello, M., Walls, A.C., Tortorici, M.A., Bianchi, S., Jaconi, S., Culap, K., Zatta, F., De Marco, A., et al. (2020). Cross-neutralization of SARS-CoV-2 by a human monoclonal SARS-CoV antibody. Nature *583*, 290–295. https://doi.org/10.1038/s41586-020-2349-y.

24. Li, D., Edwards, R.J., Manne, K., Martinez, D.R., Schäfer, A., Alam, S.M., Wiehe, K., Lu, X., Parks, R., Sutherland, L.L., et al. (2021). In vitro and in vivo functions of SARS-CoV-2 infection-enhancing and neutralizing antibodies. Cell *184*, 4203–4219.e32. https://doi.org/10.1016/j.cell.2021.06.021.

25. Li, D., Sempowski, G.D., Saunders, K.O., Acharya, P., and Haynes, B.F. (2022). SARS-CoV-2 neutralizing antibodies for COVID-19 prevention and treatment. Annu. Rev. Med. *73*, 1–16. https://doi.org/10.1146/annurev-med-042420-113838.

26. Whittle, J.R.R., Zhang, R., Khurana, S., King, L.R., Manischewitz, J., Golding, H., Dormitzer, P.R., Haynes, B.F., Walter, E.B., Moody, M.A., et al. (2011). Broadly neutralizing human antibody that recognizes the receptor-binding pocket of influenza virus hemagglutinin. Proc. Natl. Acad. Sci. USA *108*, 14216–14221. https://doi.org/10.1073/pnas.1111497108.

27. Wang, Z., Muecksch, F., Cho, A., Gaebler, C., Hoffmann, H.-H., Ramos, V., Zong, S., Cipolla, M., Johnson, B., Schmidt, F., et al. (2022). Conserved neutralizing epitopes on the N-terminal domain of variant SARS-CoV-2 spike proteins. Preprint at bioRxiv. https://doi.org/10.1101/2022.02.01.478695.

28. Hastie, K.M., Li, H., Bedinger, D., Schendel, S.L., Dennison, S.M., Li, K., Rayaprolu, V., Yu, X., Mann, C., Zandonatti, M., et al. (2021). Defining variant-resistant epitopes targeted by SARS-CoV-2 antibodies: a global consortium study. Science *374*, 472–478. https://doi.org/10.1126/science.abh2315.

29. Martinez, D.R., Schäfer, A., Gobeil, S., Li, D., De la Cruz, G., Parks, R., Lu, X., Barr, M., Stalls, V., Janowska, K., et al. (2022). A broadly cross-reactive antibody neutralizes and protects against sarbecovirus challenge in mice. Sci. Transl. Med. *14*, eabj7125. https://doi.org/10.1126/scitranslmed.abj7125.

30. Yamin, R., Jones, A.T., Hoffmann, H.-H., Schäfer, A., Kao, K.S., Francis, R.L., Sheahan, T.P., Baric, R.S., Rice, C.M., Ravetch, J.V., et al. (2021). Fc-engineered antibody therapeutics with improved anti-SARS-CoV-2 efficacy. Nature *599*, 465–470. https://doi.org/10.1038/s41586-021-04017-w.

31. Tauzin, A., Nayrac, M., Benlarbi, M., Gong, S.Y., Gasser, R., Beaudoin-Bussières, G., Brassard, N., Laumaea, A., Vézina, D., Prévost, J., et al. (2021). A single dose of the SARS-CoV-2 vaccine BNT162b2 elicits Fc-mediated antibody effector functions and T cell responses. Cell Host Microbe *29*, 1137–1150.e6. https://doi.org/10.1016/j.chom.2021.06.001.

32. Bartsch, Y.C., Wang, C., Zohar, T., Fischinger, S., Atyeo, C., Burke, J.S., Kang, J., Edlow, A.G., Fasano, A., Baden, L.R., et al. (2021). Humoral signatures of protective and pathological SARS-CoV-2 infection in children. Nat. Med. *27*, 454–462. https://doi.org/10.1038/s41591-021-01263-3.

33. Chan, C.E.Z., Seah, S.G.K., Chye, D.H., Massey, S., Torres, M., Lim, A.P.C., Wong, S.K.K., Neo, J.J.Y., Wong, P.S., Lim, J.H., et al. (2021). The Fc-mediated effector functions of a potent SARS-CoV-2 neutralizing antibody, SC31, isolated from an early convalescent COVID-19 patient, are essential for the optimal therapeutic efficacy of the antibody. PLoS One *16*, e0253487. https://doi.org/10.1371/journal.pone.0253487.

34. Kaplonek, P., Fischinger, S., Cizmeci, D., Bartsch, Y.C., Kang, J., Burke, J.S., Shin, S.A., Dayal, D., Martin, P., Mann, C., et al. (2022). mRNA-1273 vaccine-induced antibodies maintain Fc effector functions across SARS-CoV-2 variants of concern. Immunity *55*, 355–365.e4. https://doi.org/10.1016/j.immuni.2022.01.001.

35. Bruhns, P., and Jönsson, F. (2015). Mouse and human FcR effector functions. Immunol. Rev. *268*, 25–51. https://doi.org/10.1111/imr.12350.

36. Agnihothram, S., Menachery, V.D., Yount, B.L., Lindesmith, L.C., Scobey, T., Whitmore, A., Schäfer, A., Heise, M.T., and Baric, R.S. (2018). Development of a broadly accessible Venezuelan equine encephalitis virus replicon particle vaccine platform. J. Virol. *92*, e00027-18. https://doi.org/10.1128/JVI.00027-18.

37. Deming, D., Sheahan, T., Heise, M., Yount, B., Davis, N., Sims, A., Suthar, M., Harkema, J., Whitmore, A., Pickles, R., et al. (2006). Vaccine efficacy in senescent mice challenged with recombinant SARS-CoV bearing epidemic and zoonotic spike variants. PLoS Med. *3*, e525. https://doi.org/10.1371/journal.pmed.0030525.

38. Leist, S.R., Dinnon, K.H., Schäfer, A., Tse, L.V., Okuda, K., Hou, Y.J., West, A., Edwards, C.E., Sanders, W., Fritch, E.J., et al. (2020). A mouse-adapted SARS-CoV-2 induces acute lung injury (ALI) and mortality in standard laboratory mice. Cell *183*, 1070–1085.e12. https://doi.org/10.1016/j.cell.2020.09.050.

39. Dinnon, K.H., Leist, S.R., Schäfer, A., Edwards, C.E., Martinez, D.R., Montgomery, S.A., West, A., Yount, B.L., Hou, Y.J., Adams, L.E., et al. (2020). A mouse-adapted model of SARS-CoV-2 to test COVID-19 countermeasures. Nature *586*, 560–566. https://doi.org/10.1038/s41586-020-2708-8.

40. Chung, A.W., Kumar, M.P., Arnold, K.B., Yu, W.H., Schoen, M.K., Dunphy, L.J., Suscovich, T.J., Frahm, N., Linde, C., Mahan, A.E., et al. (2015). Dissecting polyclonal vaccine-induced humoral immunity against HIV using systems serology. Cell *163*, 988–998. https://doi.org/10.1016/j.cell.2015.10.027.

41. Boni, M.F., Lemey, P., Jiang, X., Lam, T.T.-Y., Perry, B.W., Castoe, T.A., Rambaut, A., and Robertson, D.L. (2020). Evolutionary origins of the SARS-CoV-2 sarbecovirus lineage responsible for the COVID-19 pandemic. Nat. Microbiol. *5*, 1408–1417. https://doi.org/10.1038/s41564-020-0771-4.

42. Leist, S.R., Dinnon, K.H., Schäfer, A., Tse, L.V., Okuda, K., Hou, Y.J., West, A., Edwards, C.E., Sanders, W., Fritch, E.J., et al. (2020). A mouse-adapted SARS-CoV-2 induces acute lung injury and mortality in standard laboratory mice. Cell *183*, 1070–1085.e12. https://doi.org/10.1016/j.cell.2020.09.050.

43. DiPiazza, A.T., Leist, S.R., Abiona, O.M., Moliva, J.I., Werner, A., Minai, M., Nagata, B.M., Bock, K.W., Phung, E., Schäfer, A., et al. (2021). COVID-19 vaccine mRNA-1273 elicits a protective immune profile in mice that is not associated with vaccine-enhanced disease upon SARS-CoV-2 challenge. Immunity *54*, 1869–1882.e6. https://doi.org/10.1016/j.immuni.2021.06.018.

44. Menachery, V.D., Gralinski, L.E., Baric, R.S., and Ferris, M.T. (2015). New metrics for evaluating viral respiratory pathogenesis. PLoS One *10*, e0131451. https://doi.org/10.1371/journal.pone.0131451.

45. Geanes, E.S., LeMaster, C., Fraley, E.R., Khanal, S., McLennan, R., Grundberg, E., Selvarangan, R., and Bradley, T. (2022). Cross-reactive antibodies elicited to conserved epitopes on SARS-CoV-2 spike protein after infection and vaccination. Sci. Rep. *12*, 6496. https://doi.org/10.1038/s41598-022-10230-y.

46. Wang, C., van Haperen, R., Gutiérrez-Álvarez, J., Li, W., Okba, N.M.A., Albulescu, I., Widjaja, I., van Dieren, B., Fernandez-Delgado, R., Sola, I., et al. (2021). A conserved immunogenic and vulnerable site on the coronavirus spike protein delineated by cross-reactive monoclonal antibodies. Nat. Commun. *12*, 1715. https://doi.org/10.1038/s41467-021-21968-w.

47. Bolles, M., Deming, D., Long, K., Agnihothram, S., Whitmore, A., Ferris, M., Funkhouser, W., Gralinski, L., Totura, A., Heise, M., et al. (2011). A double-inactivated severe acute respiratory syndrome coronavirus vaccine provides incomplete protection in mice and induces increased eosinophilic proinflammatory pulmonary response upon challenge. J. Virol. *85*, 12201–12215. https://doi.org/10.1128/JVI.06048-11.

48. Murakami, S., Kitamura, T., Matsugo, H., Kamiki, H., Oyabu, K., Sekine, W., Takenaka-Uema, A., Sakai-Tagawa, Y., Kawaoka, Y., and Horimoto, T. (2022). Isolation of bat sarbecoviruses of SARS-CoV-2 clade, Japan. Preprint at bioRxiv. https://doi.org/10.1101/2022.05.16.492045.

49. Schäfer, A., Leist, S.R., Gralinski, L.E., Martinez, D.R., Winkler, E.S., Okuda, K., Hawkins, P.E., Gully, K.L., Graham, R.L., Scobey, D.T., et al. (2022). A multitrait locus regulates sarbecovirus pathogenesis. mBio *13*, e0145422. https://doi.org/10.1128/mbio.01454-22.

50. Aleebrahim-Dehkordi, E., Molavi, B., Mokhtari, M., Deravi, N., Fathi, M., Fazel, T., Mohebalizadeh, M., Koochaki, P., Shobeiri, P., and Hasanpour-Dehkordi, A. (2022). T helper type (Th1/Th2) responses to SARS-CoV-2 and influenza A (H1N1) virus: from cytokines produced to immune responses. Transpl. Immunol. *70*, 101495. https://doi.org/10.1016/j.trim.2021.101495.

51. Ackerman, M.E., Das, J., Pittala, S., Broge, T., Linde, C., Suscovich, T.J., Brown, E.P., Bradley, T., Natarajan, H., Lin, S., et al. (2018). Route of immunization defines multiple mechanisms of vaccine-mediated protection against SIV. Nat. Med. *24*, 1590–1598. https://doi.org/10.1038/s41591-018-0161-0.

52. Fischinger, S., Fallon, J.K., Michell, A.R., Broge, T., Suscovich, T.J., Streeck, H., and Alter, G. (2019). A high-throughput, bead-based, antigen-specific assay to assess the ability of antibodies to induce complement activation. J. Immunol. Methods *473*, 112630. https://doi.org/10.1016/j.jim.2019.07.002.

53. Pegu, A., O'Connell, S.E., Schmidt, S.D., O'Dell, S., Talana, C.A., Lai, L., Albert, J., Anderson, E., Bennett, H., Corbett, K.S., et al. (2021). Durability of mRNA-1273 vaccine–induced antibodies against SARS-CoV-2 variants. Science *373*, 1372–1377. https://doi.org/10.1126/science.abj4176.

54. Tan, C.S., Collier, A.R.Y., Yu, J., Liu, J., Chandrashekar, A., McMahan, K., Jacob-Dolan, C., He, X., Roy, V., Hauser, B.M., et al. (2022). Durability of heterologous and homologous COVID-19 vaccine boosts. JAMA Netw. Open *5*, e2226335. https://doi.org/10.1001/jamanetworkopen.2022.26335.

55. Bartsch, Y.C., Tong, X., Kang, J., Avendaño, M.J., Serrano, E.F., García-Salum, T., Pardo-Roa, C., Riquelme, A., Cai, Y., Renzi, I., et al. (2022). Omicron variant Spike-specific antibody binding and Fc activity are preserved in recipients of mRNA or inactivated COVID-19 vaccines. Sci. Transl. Med. *14*, eabn9243. https://doi.org/10.1126/scitranslmed.abn9243.

56. Dugan, H.L., Stamper, C.T., Li, L., Changrob, S., Asby, N.W., Halfmann, P.J., Zheng, N.-Y., Huang, M., Shaw, D.G., Cobb, M.S., et al. (2021). Profiling B cell immunodominance after SARS-CoV-2 infection reveals antibody evolution to non-neutralizing viral targets. Immunity *54*, 1290–1303.e7. https://doi.org/10.1016/j.immuni.2021.05.001.

57. Davis, N.L., Brown, K.W., and Johnston, R.E. (1996). A viral vaccine vector that expresses foreign genes in lymph nodes and protects against mucosal challenge. J. Virol. *70*, 3781–3787. https://doi.org/10.1128/jvi.70.6.3781-3787.1996.

58. Mok, H., Lee, S., Utley, T.J., Shepherd, B.E., Polosukhin, V.V., Collier, M.L., Davis, N.L., Johnston, R.E., and Crowe, J.E. (2007). Venezuelan equine encephalitis virus replicon particles encoding respiratory syncytial virus surface glycoproteins induce protective mucosal responses in mice and cotton rats. J. Virol. *81*, 13710–13722. https://doi.org/10.1128/JVI.01351-07.

59. Hawman, D.W., Meade-White, K., Archer, J., Leventhal, S.S., Wilson, D., Shaia, C., Randall, S., Khandhar, A.P., Krieger, K., Hsiang, T.-Y., et al. (2022). SARS-CoV2 variant-specific replicating RNA vaccines protect from disease following challenge with heterologous variants of concern. Elife *11*, e75537. https://doi.org/10.7554/eLife.75537.

60. Palladino, G., Chang, C., Lee, C., Music, N., De Souza, I., Nolasco, J., Amoah, S., Suphaphiphat, P., Otten, G.R., Settembre, E.C., et al. (2022). Self-amplifying mRNA SARS-CoV-2 vaccines raise cross-reactive immune response to variants and prevent infection in animal models. Mol. Ther. Methods Clin. Dev. *25*, 225–235. https://doi.org/10.1016/j.omtm.2022.03.013.

61. Erasmus, J.H., Khandhar, A.P., O'Connor, M.A., Walls, A.C., Hemann, E.A., Murapa, P., Archer, J., Leventhal, S., Fuller, J.T., Lewis, T.B., et al. (2020). An Alphavirus-derived replicon RNA vaccine induces SARS-CoV-2 neutralizing antibody and T cell responses in mice and nonhuman primates. Sci. Transl. Med. *12*, eabc9396. https://doi.org/10.1126/scitranslmed.abc9396.

62. Greaney, A.J., Loes, A.N., Gentles, L.E., Crawford, K.H.D., Starr, T.N., Malone, K.D., Chu, H.Y., and Bloom, J.D. (2021). Antibodies elicited by mRNA-1273 vaccination bind more broadly to the receptor binding domain than do those from SARS-CoV-2 infection. Sci. Transl. Med. *13*, eabi9915. https://doi.org/10.1126/scitranslmed.abi9915.

63. Min, L., and Sun, Q. (2021). Antibodies and vaccines target RBD of SARS-CoV-2. Front. Mol. Biosci. *8*, 671633.

64. Voss, W.N., Hou, Y.J., Johnson, N.V., Delidakis, G., Kim, J.E., Javanmardi, K., Horton, A.P., Bartzoka, F., Paresi, C.J., Tanno, Y., et al. (2021). Prevalent, protective, and convergent IgG recognition of SARS-CoV-2 non-RBD spike epitopes. Science *372*, 1108–1112. https://doi.org/10.1126/science.abg5268.

65. Prakash, S., Srivastava, R., Coulon, P.-G., Dhanushkodi, N.R., Chentoufi, A.A., Tifrea, D.F., Edwards, R.A., Figueroa, C.J., Schubl, S.D., Hsieh, L., et al. (2021). Genome-wide B cell, CD4+, and CD8+ T cell epitopes that are highly conserved between human and animal coronaviruses, identified from SARS-CoV-2 as targets for preemptive pan-coronavirus vaccines. J. Immunol. *206*, 2566–2582. https://doi.org/10.4049/jimmunol.2001438.

66. Sauer, M.M., Tortorici, M.A., Park, Y.-J., Walls, A.C., Homad, L., Acton, O.J., Bowen, J.E., Wang, C., Xiong, X., de van der Schueren, W., et al. (2021). Structural basis for broad coronavirus neutralization. Nat. Struct. Mol. Biol. *28*, 478–486. https://doi.org/10.1038/s41594-021-00596-4.

67. Dai, L., Zheng, T., Xu, K., Han, Y., Xu, L., Huang, E., An, Y., Cheng, Y., Li, S., Liu, M., et al. (2020). A universal design of betacoronavirus vaccines against COVID-19, MERS, and SARS. Cell *182*, 722–733.e11. https://doi.org/10.1016/j.cell.2020.06.035.

68. Cohen, A.A., Gnanapragasam, P.N.P., Lee, Y.E., Hoffman, P.R., Ou, S., Kakutani, L.M., Keeffe, J.R., Wu, H.-J., Howarth, M., West, A.P., et al. (2021). Mosaic nanoparticles elicit cross-reactive immune responses to zoonotic coronaviruses in mice. Science *371*, 735–741. https://doi.org/10.1126/science.abf6840.

69. Zhao, J., Zhao, J., Mangalam, A.K., Channappanavar, R., Fett, C., Meyerholz, D.K., Agnihothram, S., Baric, R.S., David, C.S., and Perlman, S. (2016). Airway memory CD4+ T cells mediate protective immunity against emerging respiratory coronaviruses. Immunity *44*, 1379–1391. https://doi.org/10.1016/j.immuni.2016.05.006.

70. Li, X.-N., Huang, Y., Wang, W., Jing, Q.-L., Zhang, C.-H., Qin, P.-Z., Guan, W.-J., Gan, L., Li, Y.-L., Liu, W.-H., et al. (2021). Effectiveness of inactivated SARS-CoV-2 vaccines against the Delta variant infection in Guangzhou: a test-negative case-control real-world study. Emerg. Microbes Infect. *10*, 1751–1759. https://doi.org/10.1080/22221751.2021.1969291.

71. Pouwels, K.B., Pritchard, E., Matthews, P.C., Stoesser, N., Eyre, D.W., Vihta, K.-D., House, T., Hay, J., Bell, J.I., Newton, J.N., et al. (2021). Impact of Delta on viral burden and vaccine effectiveness against new SARS-CoV-2 infections in the UK. Preprint at medRxiv. https://doi.org/10.1101/2021.08.18.21262237.

72. Puranik, A., Lenehan, P.J., Silvert, E., Niesen, M.J.M., Corchado-Garcia, J., O'Horo, J.C., Virk, A., Swift, M.D., Halamka, J., Badley, A.D., et al. (2021). Comparison of two highly-effective mRNA vaccines for COVID-19 during periods of Alpha and Delta variant prevalence. Preprint at medRxiv. https://doi.org/10.1101/2021.08.06.21261707.

73. Scobie, H.M., Johnson, A.G., Suthar, A.B., Severson, R., Alden, N.B., Balter, S., Bertolino, D., Blythe, D., Brady, S., Cadwell, B., et al. (2021). Monitoring incidence of COVID-19 cases, hospitalizations, and deaths, by vaccination status — 13 U.S. Jurisdictions, april 4–july 17, 2021. MMWR Morb. Mortal. Wkly. Rep. *70*, 1284–1290. https://doi.org/10.15585/mmwr.mm7037e1.

74. Sealy, R.E., and Hurwitz, J.L. (2021). Cross-reactive immune responses toward the common cold human coronaviruses and severe acute respiratory syndrome coronavirus 2 (SARS-CoV-2): mini-review and a murine study. Microorganisms *9*, 1643. https://doi.org/10.3390/microorganisms9081643.

75. Grobben, M., van der Straten, K., Brouwer, P.J., Brinkkemper, M., Maisonnasse, P., Dereuddre-Bosquet, N., Appelman, B., Lavell, A.A., van Vught, L.A., Burger, J.A., et al. (2021). Cross-reactive antibodies after SARS-CoV-2 infection and vaccination. Elife *10*, e70330. https://doi.org/10.7554/eLife.70330.

76. Klompus, S., Leviatan, S., Vogl, T., Mazor, R.D., Kalka, I.N., Stoler-Barak, L., Nathan, N., Peres, A., Moss, L., Godneva, A., et al. (2021). Cross-reactive antibodies against human coronaviruses and the animal coronavirome suggest diagnostics for future zoonotic spillovers. Sci. Immunol. *6*, eabe9950. https://doi.org/10.1126/sciimmunol.abe9950.

77. Dacon, C., Tucker, C., Peng, L., Lee, C.-C.D., Lin, T.-H., Yuan, M., Cong, Y., Wang, L., Purser, L., Williams, J.K., et al. (2022). Broadly neutralizing antibodies target the coronavirus fusion peptide. Science *377*, eabq3773. https://doi.org/10.1126/science.abq3773.

78. Weiskopf, D., Weinberger, B., and Grubeck-Loebenstein, B. (2009). The aging of the immune system. Transpl. Int. *22*, 1041–1050. https://doi.org/10.1111/j.1432-2277.2009.00927.x.

79. Fülöp, T., Jr., Fóris, G., Wórum, I., and Leövey, A. (1985). Age-dependent alterations of Fc gamma receptor-mediated effector functions of human polymorphonuclear leucocytes. Clin. Exp. Immunol. *61*, 425–432.

80. Simmons, S.R., Bhalla, M., Herring, S.E., Tchalla, E.Y.I., and Bou Ghanem, E.N. (2021). Older but not wiser: the age-driven changes in neutrophil responses during pulmonary infections. Infect. Immun. *89*, e00653-20. https://doi.org/10.1128/IAI.00653-20.

81. Yarbro, J.R., Emmons, R.S., and Pence, B.D. (2020). Macrophage immunometabolism and inflammaging: roles of mitochondrial dysfunction, cellular senescence, CD38, and NAD. Immunometabolism *2*, e200026. https://doi.org/10.20900/immunometab20200026.

82. Linehan, E., and Fitzgerald, D.C. (2015). Ageing and the immune system: focus on macrophages. Eur. J. Microbiol. Immunol. *5*, 14–24. https://doi.org/10.1556/EUJMI-D-14-00035.

83. Rosenthal, N., and Brown, S. (2007). The mouse ascending: perspectives for human-disease models. Nat. Cell Biol. *9*, 993–999. https://doi.org/10.1038/ncb437.

84. Sun, S.-H., Chen, Q., Gu, H.-J., Yang, G., Wang, Y.-X., Huang, X.-Y., Liu, S.-S., Zhang, N.-N., Li, X.-F., Xiong, R., et al. (2020). A mouse model of SARS-CoV-2 infection and pathogenesis. Cell Host Microbe *28*, 124–133.e4. https://doi.org/10.1016/j.chom.2020.05.020.

85. Cockrell, A.S., Yount, B.L., Scobey, T., Jensen, K., Douglas, M., Beall, A., Tang, X.-C., Marasco, W.A., Heise, M.T., and Baric, R.S. (2016). A mouse model for MERS coronavirus-induced acute respiratory distress syndrome. Nat. Microbiol. *2*, 16226. https://doi.org/10.1038/nmicrobiol.2016.226.

86. White, L.J., Sariol, C.A., Mattocks, M.D., Wahala M P B, W., Yingsiwaphat, V., Collier, M.L., Whitley, J., Mikkelsen, R., Rodriguez, I.V., Martinez, M.I., et al. (2013). An alphavirus vector-based tetravalent dengue vaccine induces a rapid and protective immune response in macaques that differs qualitatively from immunity induced by live virus infection. J. Virol. *87*, 3409–3424. https://doi.org/10.1128/JVI.02298-12.

87. Davis, N.L., West, A., Reap, E., MacDonald, G., Collier, M., Dryga, S., Maughan, M., Connell, M., Walker, C., McGrath, K., et al. (2002). Alphavirus replicon particles as candidate HIV vaccines. IUBMB Life *53*, 209–211. https://doi.org/10.1080/15216540212657.

88. Wecker, M., Gilbert, P., Russell, N., Hural, J., Allen, M., Pensiero, M., Chulay, J., Chiu, Y.-L., Abdool Karim, S.S., Burke, D.S., et al. (2012). Phase I safety and immunogenicity evaluations of an alphavirus replicon HIV-1 subtype C gag vaccine in healthy HIV-1-uninfected adults. Clin. Vaccine Immunol. *19*, 1651–1660. https://doi.org/10.1128/CVI.00258-12.

89. Lundstrom, K. (2014). Alphavirus-based vaccines. Viruses *6*, 2392–2415. https://doi.org/10.3390/v6062392.

90. Dias, A.G., Atyeo, C., Loos, C., Montoya, M., Roy, V., Bos, S., Narvekar, P., Singh, T., Katzelnick, L.C., Kuan, G., et al. (2022). Antibody Fc characteristics and effector functions correlate with protection from symptomatic dengue virus type 3 infection. Sci. Transl. Med. *14*, eabm3151. https://doi.org/10.1126/scitranslmed.abm3151.

91. Wang, T.T., Maamary, J., Tan, G.S., Bournazos, S., Davis, C.W., Krammer, F., Schlesinger, S.J., Palese, P., Ahmed, R., and Ravetch, J.V. (2015). Anti-HA glycoforms drive B cell affinity selection and determine influenza vaccine efficacy. Cell *162*, 160–169. https://doi.org/10.1016/j.cell.2015.06.026.

92. Lo, M., Kim, H.S., Tong, R.K., Bainbridge, T.W., Vernes, J.-M., Zhang, Y., Lin, Y.L., Chung, S., Dennis, M.S., Zuchero, Y.J.Y., et al. (2017). Effector-attenuating substitutions that maintain antibody stability and reduce toxicity in mice. J. Biol. Chem. *292*, 3900–3908. https://doi.org/10.1074/jbc.M116.767749.

93. Bournazos, S., and Ravetch, J.V. (2017). Fcγ receptor function and the design of vaccination strategies. Immunity *47*, 224–233. https://doi.org/10.1016/j.immuni.2017.07.009.

94. DiLillo, D.J., and Ravetch, J.V. (2015). Differential Fc-receptor engagement drives an anti-tumor vaccinal effect. Cell *161*, 1035–1045. https://doi.org/10.1016/j.cell.2015.04.016.

95. Gralinski, L.E., Ferris, M.T., Aylor, D.L., Whitmore, A.C., Green, R., Frieman, M.B., Deming, D., Menachery, V.D., Miller, D.R., Buus, R.J., et al. (2015). Genome wide identification of SARS-CoV susceptibility loci using the collaborative cross. PLoS Genet. *11*, e1005504. https://doi.org/10.1371/journal.pgen.1005504.

96. Noll, K.E., Ferris, M.T., and Heise, M.T. (2019). The collaborative cross: a systems genetics resource for studying host-pathogen interactions. Cell Host Microbe *25*, 484–498. https://doi.org/10.1016/j.chom.2019.03.009.

97. Edwards, C.E., Yount, B.L., Graham, R.L., Leist, S.R., Hou, Y.J., Dinnon, K.H., Sims, A.C., Swanstrom, J., Gully, K., Scobey, T.D., et al. (2020). Swine acute diarrhea syndrome coronavirus replication in primary human cells reveals potential susceptibility to infection. Proc. Natl. Acad. Sci. USA *117*, 26915–26925. https://doi.org/10.1073/pnas.2001046117.

98. Tostanoski, L.H., Gralinski, L.E., Martinez, D.R., Schaefer, A., Mahrokhian, S.H., Li, Z., Nampanya, F., Wan, H., Yu, J., Chang, A., et al. (2021). Protective efficacy of rhesus Adenovirus COVID-19 vaccines against mouse-adapted SARS-CoV-2. J. Virol. *95*, e0097421. https://doi.org/10.1128/JVI.00974-21.

99. Schäfer, A., Martinez, D.R., Won, J.J., Meganck, R.M., Moreira, F.R., Brown, A.J., Gully, K.L., Zweigart, M.R., Conrad, W.S., May, S.R., et al. (2022). Therapeutic treatment with an oral prodrug of the remdesivir parental nucleoside is protective against SARS-CoV-2 pathogenesis in mice. Sci. Transl. Med. *14*, eabm3410. https://doi.org/10.1126/scitranslmed.abm3410.

100. Mackin, S.R., Desai, P., Whitener, B.M., Karl, C.E., Liu, M., Baric, R.S., Edwards, D.K., Chicz, T.M., McNamara, R.P., Alter, G., et al. (2022). Fcγ receptor-dependent antibody effector functions are required for vaccine protection against infection by antigenic variants of SARS-CoV-2. Preprint at bioRxiv. https://doi.org/10.1101/2022.11.27.518117.

101. Hou, Y.J., Okuda, K., Edwards, C.E., Martinez, D.R., Asakura, T., Dinnon, K.H., Kato, T., Lee, R.E., Yount, B.L., Mascenik, T.M., et al. (2020). SARS-CoV-2 reverse genetics reveals a variable infection gradient in the respiratory tract. Cell *182*, 429–446.e14. https://doi.org/10.1016/j.cell.2020.05.042.

102. Prentiss, M., Chu, A., and Berggren, K.K. (2022). Finding the infectious dose for COVID-19 by applying an airborne-transmission model to superspreader events. PLoS One *17*, e0265816. https://doi.org/10.1371/journal.pone.0265816.

103. Brown, E.P., Dowell, K.G., Boesch, A.W., Normandin, E., Mahan, A.E., Chu, T., Barouch, D.H., Bailey-Kellogg, C., Alter, G., and Ackerman, M.E. (2017). Multiplexed Fc array for evaluation of antigen-specific antibody effector profiles. J. Immunol. Methods *443*, 33–44. https://doi.org/10.1016/j.jim.2017.01.010.

104. Lofano, G., Gorman, M.J., Yousif, A.S., Yu, W.-H., Fox, J.M., Dugast, A.-S., Ackerman, M.E., Suscovich, T.J., Weiner, J., Barouch, D., et al. (2018). Antigen-specific antibody Fc glycosylation enhances humoral immunity via the recruitment of complement. Sci. Immunol. *3*, eaat7796. https://doi.org/10.1126/sciimmunol.aat7796.

105. Narowski, T.M., Raphel, K., Adams, L.E., Huang, J., Vielot, N.A., Jadi, R., de Silva, A.M., Baric, R.S., Lafleur, J.E., and Premkumar, L. (2022). SARS-CoV-2 mRNA vaccine induces robust specific and cross-reactive IgG and unequal neutralizing antibodies in naive and previously infected people. Cell Rep. *38*, 110336. https://doi.org/10.1016/j.celrep.2022.110336.

STAR★METHODS

KEY RESOURCES TABLE

REAGENT or RESOURCE	SOURCE	IDENTIFIER
Antibodies		
Anti-mouse IgG1-PE	Southern Biotech	1144–09; RRID:AB_2794641
Anti-mouse IgG2a-PE	Southern Biotech	1155-09L; RRID:AB_2794651
Anti-mouse IgG2b-PE	Southern Biotech	1186-09L; RRID:AB_2794690
Anti-mouse IgG3-PE	Southern Biotech	1191-09L; RRID:AB_2794697
Anti-mouse IgM-PE	Southern Biotech	1021–09; RRID:AB_2794243
Anti-CD66b Pac Blue	BioLegend	305112
Anti-CD3	BD Biosciences	558117; RRID:AB_397038
Anti-CD16	BD Biosciences	557758; RRID:AB_396864
Anti-CCL4	BD Biosciences	550078
Anti-C3b	MP Biomed	855385
Anti-mouse IgG	Invitrogen	A16072; RRID:AB_2534745
Mouse anti-VEE polyclonal sera	Internally generated	N/A
SARS-CoV-2 Spike S2 polyclonal antibody	Invitrogen	PA5-114534; RRID:AB_2890594
Bacterial and virus strains		
SARS-CoV-2 MA10	Leist et al.[38]	GenBank: MT952602
icSARS-CoV-2 nLuc	Dinnon et al.[39]	GenBank: MT844089
icHKU3 SRBD MA	Becker et al.[11]	GenBank: FJ211860
icSHC014-based viruses	Martinez et al.[13]	N/A
NEB® 5-alpha Competent *E. coli*	New England Biolabs	C2987
Chemicals, peptides, and recombinant proteins		
SARS-CoV-2 WT Spike	Sino Biological	40589-V08H4
SARS-CoV-2 D614G Spike	Sino Biological	40589-V08H8
SARS-CoV-2 WT S1 Domain	Sino Biological	40591-V08H
SARS-CoV-2 WT Receptor Binding Domain (RBD)	Sino Biological	40592-V08H
SARS-CoV-2 WT S2 Domain	Sino Biological	40590-V08B
SARS-CoV-2 WT N-terminal Domain	Sino Biological	40591-V49H
SARS-CoV-2 Alpha Variant S	Sino Biological	40589-V08B6
SARS-CoV-2 Beta Variant S	Sino Biological	40589-V08B7
SARS-CoV-2 Delta Variant S	Sino Biological	40589-V08B16
SARS-CoV-2 Omicron Variant S	Sino Biological	40589-V08H26
Human Coronavirus OC43 S	Sino Biological	40607-V08B
Human CoV HKU1 S (isolate N5)	Sino Biological	40606-V08B
Human Cytomegalovirus (HCMV) Glycoprotein B (gB)	Sino Biological	10202-V08H1
Human Coronavirus 229E Spike	Sino Biological	40605-V08B
SARS-CoV-1 Spike	Sino Biological	40634-V08B
PE-Streptavidin	Agilent Technologies	PB32-10
Guinea Pig Complement	Cedarlane	CL4051
Protein Transport Inhibitor	BD Biosciences	554724
Brefeldin A	Sigma	B7651
3,3′,5,5′-Tetramethylbenzidine (TMB) Liquid Substrate	Sigma-Aldrich	T0440
Non-Animal Protein-BLOCKER™ in TBS	G-Biosciences	786-190T

(*Continued on next page*)

Continued

REAGENT or RESOURCE	SOURCE	IDENTIFIER
TRIzol Reagent	ThermoFischer	15596026
Critical commercial assays		
Bio-Plex Pro Mouse Cytokine 23-Plex Immunoassay	Bio-Rad	M60009RDPD
Nano-Glo Luciferase Assay System	Promega	N1110
Experimental models: Cell lines		
Vero E6 (C1008)	American Type Culture Collection	CRL-1586
BHK21	American Type Culture Collection	CCL-10
Experimental models: Organisms/strains		
Female BALB/cAnNHsd mice	Envigo	Strain 047
Female FcR Knockout BALB/cAnNTac mice	Taconic	Model 584
Female BALB/cAnNTac mice	Taconic	Model BALB
Oligonucleotides		
SARS-CoV-2	Sequence obtained from NCBI, ordered custom gBlock from IDT	GenBank: MT020880.1
RaTG13	Sequence obtained from NCBI, ordered custom gBlock from IDT	GenBank: MN996532.2
SARS-CoV	Sequence obtained from NCBI, ordered custom gBlock from IDT	GenBank: AY278741
SHC014	Sequence obtained from NCBI, ordered custom gBlock from IDT	GenBank: KC881005.1
WIV1	Sequence obtained from NCBI, ordered custom gBlock from IDT	GenBank: KC881007.1
HKU3	Sequence obtained from NCBI, ordered custom gBlock from IDT	GenBank: FJ211859.1
NL63	Sequence obtained from NCBI, ordered custom gBlock from IDT	GenBank: AY567487.2
OC43	Sequence obtained from NCBI, ordered custom gBlock from IDT	GenBank: UDM84911.1
229E	Sequence obtained from NCBI, ordered custom gBlock from IDT	GenBank: KY621348.1
HKU1	Sequence obtained from NCBI, ordered custom gBlock from IDT	GenBank: HM034837.1
Recombinant DNA		
pVR21 replicon constructs	Internally generated using nucleotides listed above	N/A
Software and algorithms		
GraphPad PRISM 9	GraphPad Software, LLC	Site license
R Studio V 1.4.1103	RStudio, PBC	Open Source
FlowJo V. 10.8	FlowJo, LLC	www.flowjo.com/solutions/flowjo/downloads
systemsseRology pipeline	Github	https://github.com/LoosC/systemsseRology
Other		
NHS-Sulfo-LC-LC Kit	ThermoFisher	21435
Zebra-Spin Desalting and Chromatography Columns	ThermoFisher	89882
Fix & Perm Cell Permeabilization Kit	ThermoFisher	GAS002S-100
iQue Forecyt	Sartorius	60028
iQue Screener Plus	Intellicyt/Sartorius	11811
384-well HydroSpeed Plate Washer	Tecan	30190112
MagPlex Microspheres	Luminex MFG	MC12001-01

(*Continued on next page*)

Continued

REAGENT or RESOURCE	SOURCE	IDENTIFIER
Green Fluorescent Neutravidin Microspheres	ThermoFisher	F8776
Red Fluorescent Neutravidin Microspheres	ThermoFisher	F8775
T7 mMessage mMachine	Invitrogen	AM1344
SpectraMax ABS Plus Absorbance ELISA Microplate Reader	Molecular Devices	https://www.moleculardevices.com/products/microplate-readers/absorbance-readers
Whole body plethysmography (BUXCO)	DSI Buxco Respiratory Solutions, INC	https://www.datasci.com/products/buxco-respiratory-products/finepointe-whole-body-plethysmography
MAGPIX	Luminex	https://www.luminexcorp.com/magpix-system/

RESOURCE AVAILABILITY

Lead contact

Further information and requests for resources and reagents should be directed to and will be fulfilled by the lead contact, Lily Adams (ladams@med.unc.edu), or corresponding author Ralph Baric (rbaric@email.unc.edu) upon material transfer agreement.

Materials availability

Unless stated, VRP spike vaccines and coronaviruses included in this study are available upon request, with satisfaction of biosafety requirements, and completion of material transfer agreement. SARS-CoV-2 MA10 is commercially available from BEI resources under item number NR-55329.

Data and code availability

Animal challenge and *in vitro* raw data is available from the lead contact upon request.

Code used in this study is available on the GitHub code repository under https://github.com/LoosC/systemsseRology. Code specific for the analyses in this study have also been included as a supplemental file and are available under https://doi.org/10.5281/zenodo.7621099.

Any additional information required to reanalyze the data reported in this paper is available from the lead contact upon request.

EXPERIMENTAL MODEL AND SUBJECT DETAILS

Biosafety and institutional approval

All experiments were conducted after approval from the UNC Chapel Hill Institutional Biosafety Committee and Institutional Animal Care and Use Committee according to guidelines outlined by the Association for the Assessment and Accreditation of Laboratory Animal Care and the US Department of Agriculture. All vaccinations were performed at ABSL2 while all infections and downstream assays were performed at ABSL3 in accordance with Environmental Health and Safety. All work was performed with approved standard operating procedures and safety conditions for SARS-CoV-2. Our institutional ABSL3 facilities have been designed to conform to the safety requirements recommended by Biosafety in Microbiological and Biomedical Laboratories (BMBL), the US Department of Health and Human Services, the Public Health Service, the Centers for Disease Control and Prevention (CDC), and the National Institutes of Health (NIH). Laboratory safety plans have been submitted, and the facility has been approved for use by the UNC Department of Environmental Health and Safety (EHS) and the CDC.

Cell lines

Vero E6 cells used in this study were obtained from the American Type Culture Collection (ATCC) and have been maintained in our laboratory. Cells were maintained in Dulbecco's Modified Eagle's Medium (DMEM) supplemented with 5% FBS and anti/anti. Vero E6 cells were used to recover and propagate virus as well as *in vitro* assays. Baby Hamster Kidney (BHK21) cells were obtained from ATCC and maintained in our laboratory. Cells were maintained in α -MEM supplemented with 10% fetal bovine serum, L-glutamine, and 10% tryptose phosphate broth. BHK21 cells were used to build VRP vaccines. All cells were maintained at 37C under 5% CO_2. Cells were not authenticated prior to use. Cells were confirmed mycoplasma-free prior to use.

Animal models

Female BALB/c mice were used in this study, obtained from both Envigo and Taconic for substrain purposes detailed further. Female mice show consistent coronavirus disease phenotypes and are the gender used in standard models like those described in this

manuscript. Mice were randomly assigned to cages in groups of 3–5 mice per cage, fed a standard rodent laboratory diet, and housed under standard temperature and environmental conditions. Female BALB/cAnNHsd were obtained from Envigo (strain 047) and delivered at either 8–10 weeks (young) or 11–12 months (old). Female FcR-knockout mice were obtained from Taconic (Model 584), on a BALB/cAnNTac background delivered at 6–10 weeks old due to strain availability. Age-matched strain specific counterparts (Female BALB/cAnNTac) were also obtained from Taconic.

Viruses

All viruses were confirmed mycoplasma-free prior to use, and all viruses were subjected to next-generation sequencing prior to use to confirm sequence identity. Mouse adapted SARS-CoV-2 MA10[42] and SARS-CoV-2 nanoLuciferase reporter viruses were developed based on the SARS-CoV-2 WA1 reference strain[101] and propagated from a cDNA molecular clone as previously described. Mouse adapted bat virus HKU3 was generated from a cDNA molecular clone[11,49] and mutations were inserted that cause pathogenesis in mice. To generate the SARS-CoV-2 spike domain panel, the backbone sequence from bat virus SHC014[4] was used. SHC014 spike sequences were replaced with corresponding fragments of the sequence encoding SARS-CoV-2 spike segments (RBD, RBD+, NTD, RBD-NTD, S1) and viruses were generated from the cDNA clone.

METHOD DETAILS

VEE VRP3526 vaccine preparation

The sequence encoding CoV spike proteins (below) were cloned into the pVR21 vector containing Venezuelan equine encephalitis virus strain 3526 non-structural proteins. RNA from template pVR21 constructs and VEE 3526 helper constructs encoding glycoprotein and capsid proteins was transcribed using Invitrogen T7 mMessage mMachine*in vitro* transcription kit. Purified RNA was electroporated into BHK21 cells in the ratio of 2:1:1 pVR21 construct: VEE 3526 glycoprotein: capsid. Supernatant was harvested and purified 24 h post-electroporation and ultracentrifuge concentrated through sucrose cushion. VRP titers were determined through immunofluorescent staining to detect VEE-associated proteins. All VRPs were confirmed to not cause cytopathic effect in cell culture before administration to mice.

Mice, vaccination, and infection

Prior work indicates that group sizes of five to ten mice is sufficient to evaluate significance within a half-log.[39,42] Mice were vaccinated with 2×10^4 VRP in a 10 μL phosphate-buffered saline footpad inoculation and boosted with the same dose 3 weeks post-prime. Baseline, pre-boost, and pre-challenge serum was collected via submandibular bleed. Four weeks post-boost, mice were infected with 10^3 or 10^4 (where specified) PFU SARS-CoV-2 MA10 or 10^5 PFU HKU3 MA-SRBD in 50 μL PBS intranasally under ketamine-xylasine anesthesia. The challenge doses were at least one log higher than the suspect infectious dose in humans.[102] For adoptive and passive transfer experiments, 200 μL serum from vaccinated mice was transferred to naive mice via intraperitoneal injection 24 h prior to challenge. Mice were weighed daily through the course of infection, and a subset's respiratory function was tracked daily using whole body plethysmography.[44] Mice were euthanized at 2 and 5 days post infection via isoflurane overdose. The relevant infectious challenge dose for FcR knockout mice was determined to be 10^3 PFU SARS-CoV-2 MA10 due to strain-specificities, and mice were infected and monitored as described above.

Mouse tissue collection and analysis

After euthanasia, blood was collected into phase separation tubes by cardiocentesis or severing the vena cava and allowed to clot before centrifugation to separate serum. Lungs were scored for gross discoloration, indicating congestion and/or hemorrhage, based on a semi-quantitative scale of mild to severe discoloration covering 0 to 100% of the lung surface. The left lung was collected and injected with 10% neutral buffered formalin to expand airways before storage in fixative for 7 days before histopathological processing. Of the right lung lobes, the inferior lobe was collected in ~1 mL TRIzol reagent with glass beads and the superior lobe was collected in ~1 mL phosphate buffered saline with glass beads. Both inferior and superior lobes were homogenized in a MagnaLyser and debris was pelleted. Virus in the lungs was quantified from the superior lobe via plaque assay. Briefly, virus was serial diluted and inoculated onto confluent monolayers of Vero E6 cells, followed by agarose overlay. Plaques were visualized on day 2 post infection via staining with neutral red dye. Lung cytokines were quantified from the superior lobe using the Bio-Plex Pro Mouse Cytokine 23-Plex Immunoassay. RNA from the inferior lobe was reserved for additional downstream assays.

Neutralization assays

A serial dilution (1:20 initially, followed by a 3-fold dilution) of pre-challenge serum was incubated in a 1:1 ratio with SARS-CoV-2-nLuc[101] to result in 800 PFU virus per well. Serum-virus complexes were incubated at 37C with 5% CO2 for 1 h. Following incubation, serum-virus complexes were added to a confluent monolayer of Vero E6 cells and incubated for 48 h at 37C with 5% CO_2. After incubation, luciferase activity was measured with the Nano-Glo Luciferase Assay System (Promega) according to the manufacturer specifications. Neutralization titers (ID50) were defined as the dilution at which a 50% reduction in RLU was observed relative to the virus (no antibody) control.

Systems serology

SARS-CoV-2 and other sarbecovirus and control antigens were resuspended in water to a final concentration of 0.5 mg/mL and linked to magnetic Luminex beads (Luminex Corp, TX, USA) through carbodiimide NHS ester linkages. Specific antigens were coupled to individual bead regions. Biotinylation of antigens were done using the NHS-Sulfo-LC-LC kit, and excess biotin was removed using Zebra-Spin desalting and size exclusion columns. Antigen coupled beads were then incubated with serum at various dilutions (1:100 for IgG2a, IgG2b, IgG3, IgM, 1:200 for IgG1, and 1:750 for Fcγ-receptor binding) in a 384-well plate (Greiner, Germany) overnight at 4°C. Unbound material was washed and detection of isotypes and subclasses were done using PE-conjugated anti-IgG1, -IgG2a, -IgG2b, -IgG3, -IgM. PE-Streptavidin (Agilent Technologies, CA, USA) was coupled to recombinant and biotinylated mouse FcγR2b, FcγR3, and FcγR4A at a 1:1000 dilution. Secondary detection was done at room temperature for 1 h, and unbound material was removed by washing. Relative binding per antigen was determined on an IQue Screener PLUS cytometer (IntelliCyt).

Antibody-dependent cellular phagocytosis (ADCP) and neutrophil phagocytosis (ADNP) assays were done as previously described.[103] Mouse serum was incubated with cultured monocytes or primary neutrophils at a concentration of 1:100 on preformed immune complexes on fluorescent neutravidin microspheres. Cells were fixed with 4% paraformaldehyde (PFA) and identified by gating on microsphere-positive cells. Phagocytic score was quantified by the (percentage of microsphere-positive cells) x (MFI of microsphere-positive cells) divided by 100000. Antibody-dependent complement deposition (ADCD) was done as previously described.[104] Relative complement deposition was quantified through flow cytometry, as measured by fluorescein-conjugated goat IgG that targets the guinea pig complement C3b.

Enzyme-linked immunosorbent assay

All serum samples tested by ELISA assay were heat-inactivated at 56°C for 30 min to reduce risk from possible residual virus in serum. ELISA binding titer for full-length spike protein was measured as described before.[105] Full-length spike protein at 2 μg/mL in Tris-Buffered Saline (TBS) pH 7.4 was coated in the 96-well microtiter plate for 1 h at 37°C. The wells were blocked with 3% milk in TBS containing 0.05% Tween 20 (TBST) for 1 h, then serially diluted serum samples were added (1:100–1:24,300) to the wells and incubated for an additional hour at 37°C. The plate was washed three times using wash buffer (TBS containing 0.2% Tween 20), then goat anti-mouse IgG (Catalog # A16072) was added at 1:2000 and incubated for 1 h at 37°C. The plate was washed three times using wash buffer, then 3,3′,5,5′-Tetramethylbenzidine (TMB) Liquid Substrate (Sigma-Aldrich) was added to the plate, and absorbance was measured at 450 nm using a plate reader (Molecular Devices SpectraMax ABS Plus Absorbance ELISA Microplate Reader) after stopping the reaction with 1 N HCl. ELISA binding titer for Spike RBD or NTD was measured as described above with minor modifications. 96-well microtiter plate was coated with Streptavidin (Invitrogen) at 4 μg/mL in TBS pH 7.4 for 1 h at 37°C. The wells were blocked with 1:1 Non-Animal Protein-BLOCKER (G-Biosciences) in TBS for 1 h. Biotinylated spike RBD or NTD antigen (1 μg/mL) was captured onto the streptavidin-coated wells, then serially diluted serum samples (1:100–1:24,300) were added to the wells and incubated for 1 h at 37°C. The plate was washed three times using wash buffer (TBS containing 0.2% Tween 20), then goat anti-mouse IgG (Catalog # A16072) was added at 1:2000 and incubated for 1 h at 37°C. The plate was washed three times using wash buffer, then 3,3′,5,5′-Tetramethylbenzidine (TMB) Liquid Substrate (Sigma-Aldrich) was added to the plate, and absorbance was measured at 450 nm using a plate reader (Molecular Devices SpectraMax ABS Plus Absorbance ELISA Microplate Reader) after stopping the reaction with 1 N HCl.

QUANTIFICATION AND STATISTICAL ANALYSIS

Systems serology

An initial multivariate discriminate analysis (partial least squares discriminant analysis, or PLS-DA) was conducted to evaluate whether the serological characteristics can differentiate between baseline and post-boost groups as well as predict the minimal distinguishing features that can differentiate between groups. Features were selected via least absolute shrinkage and selection operator (LASSO) as previously described,[51] classified using a fold-specific support vector machine (SVM) classifier, and the PLS-DA was used to visualize the variables identified and classified. To obtain optimal resolution on feature identification and validate our findings, we ran two models that included (1) Ig subclass and functional assays and (2) FcR affinity and functional assays. We also ran validations via randomization to confirm that the LASSO/SVM could significantly differentiate selected features from randomly selected features and permutations. Correlations between Fab, FcR, and functional assays were done using GraphPad Prism using Spearman's coefficients. Statistical significance, as defined by $p < 0.05$, was corrected for multiple comparisons using Benjamini-Hochberg correction. Other analyses such as PLS-DA were done on R using the systemsseRology pipeline available on GitHub (https://github.com/LoosC/systemsseRology) Machine learning tools (for the analysis of systems serology data) are also available. Each assay contained pre-immune and post-vaccination sera, as well as PBS controls to account for batch effects. All other calculations are described below.

Other statistical testing

All statistical analyses were conducted in GraphPad PRISM 9. Exact group numbers (n) of mice, experimental replicates, and technical replicates are noted and described in each figure legend. To assess the statistical significance of weight loss, significance was

calculated by two-way ANOVA comparing each spike vaccinated group to the GFP control. In cases where mortality was observed, significance was calculated via Mixed-effects analysis The significance of virus and antibody titers was calculated via one-way ANOVA comparing each spike vaccinated group to the GFP control. To assess the significance of lung discoloration and histopathological lung damage scoring, significance was calculated via Brown-Forsythe and Welch's ANOVA. To assess the significance of lung function (whole body plethysmography), significance between groups was calculated by Kruskal-Wallis and corrected by Dunn's multiple comparisons test. In all other cases, testing was corrected for multiple comparisons using Dunnett's multiple comparisons test, Dunnett's T3 test when total samples <50. Significance reported as *$p < 0.05$, **$p < 0.01$, ***$p < 0.001$, ****$p < 0.0001$.